AN ABSTRACT OF THE THESIS OF

Connor J. Smith for the degree of Master of Science in Chemical Engineering presented on November 22, 2013

Title: Continuous Microwave Extraction of Peppermint Oil

Abstract approved:

David E. Hackleman

Steam distillation has been the common method of extraction of essential oils from plants for more than a century. The use of microwave energy has been suggested as an alternative distillation method that would: reduce water usage, dependence on non-renewable energy sources, and the carbon footprint. A byproduct of this technique was first discovered in 2009; the creation of an aerosol, which are extremely difficult to condense with the traditional tube and shell heat exchangers used by mint farmers. Therefore, a direct-contact spray condenser was developed, tested, and proven adequate at condensing an artificially produced steam/air aerosol on the lab scale. The objective of this research is to utilize the direct-contact condenser in conjunction with an industrial scale (75 [kW]) continuous microwave drier to prove that a multi-ton level microwave extraction process is possible. A pilot scale field trial was conducted in Iowa in September 2012 with a 75 [kW] microwave unit. Practically all of the peppermint oil was extracted from the hay by the microwave application process. The direct-contact condenser and recycled condensate cooling system did not allow recoverable oil to be obtained due to the solubility of the mint oil in the cooling water. The water in the recycled condensate cooling system did contain approximately 0.45% menthol by weight, the main component of peppermint oil, and offers insight into potential improvements to the condensation process to achieve microwave extraction of peppermint oil at the mint hay multi-ton level of operation.

Continuous Microwave Extraction of Peppermint Oil

by
Connor J. Smith

A THESIS

submitted to

Oregon State University

in partial fulfillment of
the requirements for the
degree of

Master of Science

Presented November 22, 2013

Commencement June 2014

Master of Science thesis of Connor J. Smith presented on November 22, 2013

APPROVED:

Major Professor, representing Chemical Engineering

Head of the School of Chemical, Biological and Environmental Engineering

---

Dean of the Graduate School

I understand that my thesis will become part of the permanent collection of Oregon State University libraries. My signature below authorizes release of my thesis to any reader upon request.

Connor J. Smith, Author

ACKNOWLEDGEMENTS

I thank Dr. David Hackleman for guidance and mentorship throughout this research. Jonathan Lebsack set the foundation for my research, has been an invaluable resource, and even traveled all the way to Nevada, Iowa, with Dr. Hackleman and me during the summer of 2012.

I also thank Newhouse Manufacturing in Redmond, Oregon, for generous donation of a separator for use in the Iowa trials. This research would not have been possible without the continued dedication of Mint Industry Research Council members. John Reerslev (Reerslev Farms) donated over one thousand pounds of peppermint plant material from his farm in Junction City, Oregon. Peter O'Daniel (IP Callison & Sons) traveled to Iowa from Indiana for the experimental trials. Dale Thacker (Thacker Farms, Canada) provided helpful insight into energy efficient mint farming from the copious data he has gathered from his farm in Canada. Richard Mattix of the Hyslop Crop Science Field Research Laboratory generously allowed our group to store peppermint plant material in their industrial freezer to preserve the plants. Brian Jansen of the Oregon State University Mechanical, Industrial, and Manufacturing Engineering department and his team provided key alterations to the direct-contact condenser on short notice, without which the research would not have been possible. Cellencor™ members Ken Kaplan and Mike Mittman, and AMTek™ Microwaves representative Stephen Rogers made this research possible with the use of their equipment and technical expertise during experimentation in Iowa. Lechler Nozzles, specifically Zeke Brown, provided an extremely valuable tool to condenser and spray characteristic analysis. Justin Chi assisted in capturing high speed photographs of the spray nozzle droplets.

I thank Dr. Philip Harding for his generosity, mentorship, friendship, and immense feedback during the drafting of this document and throughout my time at Oregon State. Finally, I thank two very important people for being my support system throughout this whole process; Elisha Brackett and Cassandra Loren. I could not have completed this project without their unwavering support and encouragement.

TABLE OF CONTENTS

Page

LIST OF FIGURES

LIST OF FIGURES (Continued)

LIST OF TABLES

LIST OF APPENDIX FIGURES

NOMENCLATURE

Parameter	*Description*	*Value*	*Units*
a	Attractive van der Waals parameter	-	-
A	Heat transfer surface are	-	[m^2]
A_d	Interfacial droplet area per volume	-	[1/m]
$\alpha(T)$	Polarizability of molecule	-	-
b	Molecule size van der Waals parameter	-	-
CO_2e	Carbon dioxide equivalent	-	[kg]
C_p	Specific heat capacity	-	[J/(kg*K)]
D_{32}	Sauter mean diameter (SMD)	261	[µm]
D_c	Cyclone chamber diameter	-	[m]
D_{hay}	Hay depth on conveyor	2	[in]
D_i	Middle drop diameter in size range *i*	-	[m]
d_{pi}	Particle diameter of size range *i*	-	[µm]
$D_{p,th}$	Particle diameter where 50 % are collected	-	[µm]
E_o	Cyclone efficiency at low loading	-	[%]
ε	DCC void space	-	-
η	Condenser recovery efficiency	-	[%]
f_i^{ideal}	Pure species fugacity of liquid species *i*	-	[Pa]
$\hat{f}_i^l$	Partial molar fugacity of liquid species *i*	-	[Pa]
$\hat{f}_i^v$	Partial molar fugacity of vapor species *i*	-	[Pa]
f_i^v	Pure species fugacity of vapor species *i*	-	[Pa]
h	Convective heat transfer coefficient	-	[W/(m*K)]
ΔH_{vap}	Enthalpy of vaporization	-	[kJ/kg]
k	Thermal conductivity	-	[W/(m*K)]
κ	Peng-Robinson equation of state parameter	-	-
L	Characteristic length	-	[m]
LHV	Low heating value	-	[GJ/kg]
$\dot{m}$	Mass flow rate	-	[kg/s]
MC_{before}	Inlet hay moisture content	35	[%]
M_i	Molecular weight of species *i*	-	[g/mole]
$\dot{m}_{spraybar}$	Spray bar mass flow rate	1.1	[kg/min]
μ_g	Gas viscosity	-	[kg/(m*s)]
N	# of nozzles in use on direct-contact condenser	16	[nozzles]
n_i	Moles of species *i*	-	[moles]
N_i	Drop number is size range *i*	-	-
N_s	Effective number of gas spiral paths within cyclone	-	-

NOMENCLATURE (Continued)

Parameter	*Description*	*Value*	*Units*
Nu	Nusselt number	-	-
ω	Acentric (non-sphericity) factor	-	-
P	Total system pressure	-	[Pa]
P_c	Critical pressure	-	[K]
ϕ_d	Droplet volume fraction, or holdup	-	-
P_i^{sat}	Saturated vapor pressure of liquid species *i*	-	[Pa]
P_{MW}	Applied microwave power	60	[kW]
$\dot{q}$	Heat transfer rate	-	[W]
R	Ideal gas constant	-	[J/(mol*K)]
$R_{exhaust}$	DCC exhaust radius	-	[m]
RH	Relative humidity	-	[%]
ρ_g	Gas density	-	[kg/m^3]
ρ_p	Particle density	-	[kg/m^3]
ρ_{sat}	Saturation vapor density	-	[g/m^3]
t	Time	-	[min]
T	Total system temperature	-	[K]
T_{bp}	Bubble point temperature	-	[K]
T_c	Critical temperature	-	[K]
$T_{c,i}$	Initial cooling water temperature	17	[°C]
T_r	Reduced temperature	-	-
ΔT	Temperature difference	-	[K]
ΔT_{lm}	Log mean temperature difference	-	[K]
U	Overall heat transfer coefficient	-	[W/(m*K)]
v	Partial molar volume	-	[m^3/mol]
v_{belt}	Conveyor speed	12	[in/min]
$\dot{V}_{exhaust}$	DCC exit vapor volumetric flow	-	[m^3/s]
$v_{exhaust}$	DCC exit vapor velocity	-	[m/s]
v_{max}	Maximum cyclone velocity	-	[m/s]
V_{tank}	Water volume in cooling tank	30	[gal]
W_{hay}	Hay width on conveyor	24	[in]
x_i	Liquid mole fraction	-	-
y_i	Vapor mole fraction	-	-
Y_w	Specific humidity	-	$\left[\frac{kg\ steam}{kg\ total}\right]$

ABBREVIATIONS

Abbreviation	*Description*
BHP	Boiler horsepower
DCC	Direct-contact condenser
EOS	Equation of state
GC	Gas chromatography
GWP	Global warming potential of greenhouse gas
IR	Infrared
NG	Natural gas
RTD	Resistance temperature detector
SEM	Scanning electron microscope
SFME	Solvent-free microwave extraction
VFD	Variable frequency drive

Continuous Microwave Extraction of Peppermint Oil

1. Introduction

Essential oils have been used for centuries in food preservation, treating illness, and as a natural insecticide.[1] Specifically, peppermint oil is used in dental products, natural remedies, cosmetic fragrances, and consumer product flavoring.[1] For example, peppermint grown in the Oregon Willamette Valley produces oil that goes directly into Colgate™ Toothpaste.

Peppermint oil has been extracted via steam distillation for over a century, especially in Oregon.[2] The process is performed in batch systems with correspondingly low energy utilization. Traditional steam distillation is undesirable for several reasons. The energy released during fossil fuel combustion is utilized to produce steam from regional ground water using industrial boilers, thus emitting greenhouse gases. Boiler feed water must be chemically treated to prevent hard water scale and fouling, potentially decreasing oil quality and introducing ppm-level harsh chemical compounds into the wastewater stream. Common chemicals used to treat the feed water include neutralizing amines (e.g. cyclohexylamine) to decrease alkalinity, phosphates (e.g. sodium polyphosphate) to decrease iron build-up, chelants (e.g. ethylenediamine tetraacetic acid) to decrease water "hardness", and oxygen scavengers (e.g. sodium sulfite) to decrease equipment corrosion.[3] These chemicals then become a part of the steam that passes through the mint hay and can end up as a component of the recovered oil. Potable water is oriented in a single-pass configuration, inherently consuming copious amounts of water each harvesting season. Capitally intense, special purpose mint trailers can sit at the distillation facility for nearly two hours for the steam injection period. The connection and disconnection of these trailers to the steam system is a frequent safety risk to operators. Efficiency upgrades have been introduced; some as simple as insulating mint trailers and steam pipes to decrease heat transfer to the surroundings.

Most installed boilers employed in the peppermint industry burn diesel or natural gas. Associated costs have been and will continue to rapidly grow as natural resources are depleted. Hot water, carbon dioxide and other exhaust gas emissions are now under regulatory control in some areas. Customers of the essential oil produced by the agri-

business are driven by end user environmental awareness and seek to certify their products as "carbon neutral" if at all practical. Significant process changes must be made to provide a more sustainable product and maintain economic viability. The first of these changes would be to transform peppermint oil extraction into a continuous process, thereby improving process control and scalability. Transitioning from a batch to a continuous process requires a fundamental change to the oil extraction mechanism.

Dr. David Hackleman proposed solvent-free microwave extraction (SFME) as a technique that provides opportunity for increased sustainability and improvements in energy efficiency. First demonstrated with basil, garden mint, and thyme; SFME is a viable extraction alternative promising decreased fossil fuel dependency and increased energy efficiency.[4] SFME provides a continuous process, decreased water usage, higher energy efficiency, environmental sustainability, decreased residence time, and higher oil yields.

The open ends of industrial microwaves used in pilot-scale extractions introduce air to the system, creating challenges in the condensation step of the process. Air creates an insulating layer on the tube walls of traditional tube and shell heat exchangers. A more efficient mode of capturing volatilized oils is required. A direct-contact condenser, modeled after a common spray scrubber,[5] has been demonstrated as a plausible solution to the condensation issues present in the tube and shell model. This research investigates the use of a direct-contact condenser on a "farm-scale" continuous flow microwave system and works towards characterizing this process. Two previous in-field pilot scale tests had been performed to date; one in Stayton, Oregon, at an existing peppermint farm and another in North Carolina at an industrial microwave manufacturer facility.[6,7] The use of the direct-contact condenser did not resolve the condensation issues in the presence of air when implemented on the pilot-scale microwave system. According to Lebsack *et al.*, the direct-contact condenser should have worked effectively even at low specific humidity values (< 0.3 [kg steam/kg total]).[8]

The author seeks to understand the difference in results from that of Lebsack *et al.* The microwave vaporizes the oil and water in the plant as expected, but capture efficiency is not sufficient even with a new condenser design. Possible explanations for this include:

1. The direct-contact condenser unit may not have been able to maintain effective aerosol knockdown with the increased throughput of the microwave system (even though it was designed for a system of that scale).
    a. The number of spray nozzles and associated cooling water flow were insufficient.
2. Cooling spray and aerosol particles could have traveled through the unit too quickly, not reaching the required residence time for efficient contact, leading to entrapment in the passing air and passage through the DCC exit.
    a. Decreasing blower volumetric flow and thereby increasing aerosol residence time within the DCC could have lead to higher capture rate.
3. Steam could have been condensed in the air, creating a "fog" of liquid aerosols entrained in air, instead of vapor aerosols as was assumed initially.
    a. Condensed liquid would require a physical knockdown technique, not condensation, thereby reducing energy costs related to heat transfer.
4. The DCC only deals with gravitational separation. Introducing centrifugal acceleration with a cyclonic separation unit could lead to increased capture efficiency.
    a. Centrifugal acceleration of the aerosol particles could increase the force available for separation of the condensed steam and oil from the air.
5. Other thermodynamic and/or transport phenomena are not being considered.

2. Literature Review

2.1. Peppermint Oil

Peppermint is a specialty crop with a worldwide annual production of over 4000 metric tons, with more than 80% coming from the Northwest and Midwest United States.[9,10] Worldwide annual essential oil production from peppermint, native spearmint, cornmint (source of natural menthol), and Scotch spearmint is over 23,000 metric tons, a market value of over $400 million.[11] According to a market research study performed by IBISWorld, the United States essential oil industry profits $1.2 billion annually with annual growth of 2.6% over the past 5 years.[12] Peppermint oil from Oregon is typically used in consumer products like chewing gum, food flavoring, and cosmetic fragrances.

Peppermint plants secrete and store their oil in subcuticular storage cavities, sac-like structures, located on the underside of the leaf.[13] The oil is a toxicological defense mechanism from other plants and animals. A variety of monoterpene molecules are present in the oil and create a very strong and pungent odor and yield the distinct "minty" flavor.

Farmers traditionally sell their oil to blending and distribution companies after they have distilled it from the plant. IP Callison & Sons, located in Lacey, Washington, is an example of a supplier of essential oils from spearmint and peppermint. They buy, purify, blend, and sell mint oil from distillation facilities all over the Northwest and Midwest United States along with India and China. Consumer product companies like Wrigley's and Colgate purchase the purified oil and insert it into their chewing gum and toothpaste products, respectively. Current distillation practices do not allow for these companies to market their products as "sustainable" or "green".

2.2. Steam Distillation

Several different essential oil extraction techniques exist: water distillation, steam distillation, hydrodistillation (HD), supercritical fluid extraction, solvent-assisted extraction, ultrasonic-assisted extraction, and solvent-free microwave extraction.[14] The Oregon peppermint industry has primarily used steam distillation to extract the essential oil from the plant.[2]

Distillation Process:

The first process step involves cutting the fully grown peppermint plant near the ground. The plants are dried for several days in the field to enable mechanical processing. The plants are then chopped and a peppermint "hay" material is created. Hay is then transferred directly into a 20 x 8 x 8 [ft] mint tub trailer (sometimes called a "wagon"), creating a packed bed of mint. The trailer is then driven to the mint distillery, or "the still". Boiler steam enters the trailer through a manifold which evenly distributes the vapor through the bottom of the packed bed. Peppermint oil entrained in plant nodules on the underside of the leaf is then transported with steam, in accordance with Raoult's Law of partial pressures.[8] The vaporized water and oil are then condensed in a tube and shell condenser, separated in a conical separator, and the oil is collected and shipped to a purification facility. The condensate enters the separator at a temperature of 115 [°F] (~46 [°C]). Peppermint oil and water are most efficiently separated when their densities are dissimilar, which occurs at higher temperatures.[11] According to a study of Midwestern U.S. mint farming, 42 to 46 [°C] is the optimal temperature range for separation because it yields both the greatest difference in densities between water and peppermint oil and the least thermal degradation.[8,15]

The steam distillation process used in the 1950's, a schematic of which is shown in Figure 2.2.1, has evolved, but no major changes have been made in over 60 years.

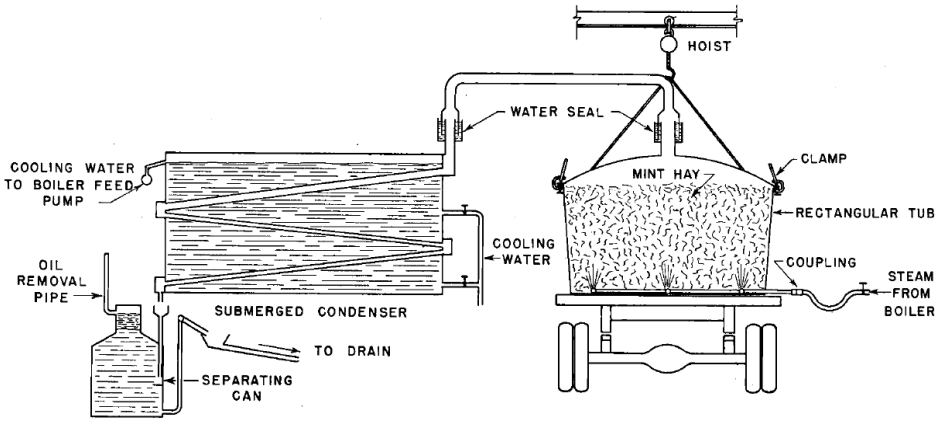

Figure 2.2.1: *1950's Steam Distillation Process*
Typical Oregon peppermint distillery in the 1950's. Temperature of cooling water out of the condenser and condensate in the separating can are monitored. Steam pressure from the boiler is changed in order to alter peppermint oil production capacity.[2]

Raoult's Law:

Fundamental analysis of the peppermint oil vaporization process is required to validate the Raoult's Law assumption. The Gibbs phase rule states that for a two-component vapor-liquid system at equilibrium the compositions of the two phases at a given temperature and pressure are not independent from each other.[16] Fugacity is a valuable tool for evaluation of vapor-liquid equilibrium problems providing a mathematical simplification of chemical potential, or partial molar free energy, μ_i. The fugacities must be equal for two components in vapor-liquid equilibrium (VLE), as shown in Equation 2.2.1:[17]

$$\hat{f}_i^v = \hat{f}_i^l, \tag{2.2.1}$$

where $\hat{f}_i^v$ is the partial molar fugacity of vapor species *i* and $\hat{f}_i^l$ is the partial molar fugacity of liquid species *i*. Equation 2.2.1 is only useful when some assumptions are made about the system and each component. The liquid and vapor can be considered ideal only when assuming low system pressure and all intermolecular forces are the same.[17] Peppermint oil is known to be less than 1% by mole of the binary mixture, i.e. dilute, and can be considered ideal. The pure species fugacity for an ideal gas is described by Equation 2.2.2:

$$\hat{f}_i^v = f_i^v = y_i P, \tag{2.2.2}$$

where f_i^v is the pure species fugacity of vapor species *i*, y_i is vapor mole fraction, and *P* is total system pressure. A reference state is chosen for an ideal liquid where all intermolecular interactions are the same. This reference state is typically known as the Lewis/Randall reference state or pure species fugacity (Equation 2.2.3):

$$\hat{f}_i^{ideal} = x_i f_i^{ideal} = x_i P_i^{sat}, \tag{2.2.3}$$

where f_i^{ideal} is the pure species fugacity of liquid species *i*, x_i is liquid mole fraction, and P_i^{sat} is the saturated vapor pressure of liquid species *i*. Combining Equations 2.2.2 and 2.2.3 leads to Raoult's Law (Equation 2.2.4):

$$y_i P = x_i P_i^{sat} \tag{2.2.4}$$

Saturated vapor pressure is a function of the system temperature, *T*. The criteria for equilibrium for a binary mixture of peppermint oil and water can be expressed by Equations 2.2.5 and 2.2.6:

$$y_p P = x_p P_p^{sat}, \tag{2.2.5}$$

$$y_w P = x_w P_w^{sat}, \tag{2.2.6}$$

where *p* and *w* represent peppermint oil and water, respectively. Total system pressure can be expressed as the sum of the two Raoult's Law expressions (Equation 2.2.7):

$$P = y_p P + y_w P = x_p P_p^{sat} + \left(1 - x_p\right) P_w^{sat} \tag{2.2.7}$$

Inserting Equation 2.2.7 into 2.2.5 leads to Equation 2.2.8:

$$y_p = \frac{x_p P_p^{sat}}{x_p P_p^{sat} + \left(1 - x_p\right) P_w^{sat}} \tag{2.2.8}$$

Binary phase diagrams can be constructed from Equations 2.2.7 and 2.2.8. by holding system pressure or temperature constant. Bubble point temperature, defined as the temperature at which the first vapor bubble forms through slow heating of a liquid at constant pressure, is useful for binary phase diagram construction.[16] Saturated vapor pressures and associated bubble point temperatures of water and peppermint oil are 760 [mm Hg], 100 [°C] and 10 [mm Hg], 215 [°C], respectively.[11,18]

Figure 2.2.2 is a graphical depiction of Raoult's Law when applied to steam distillation of peppermint.

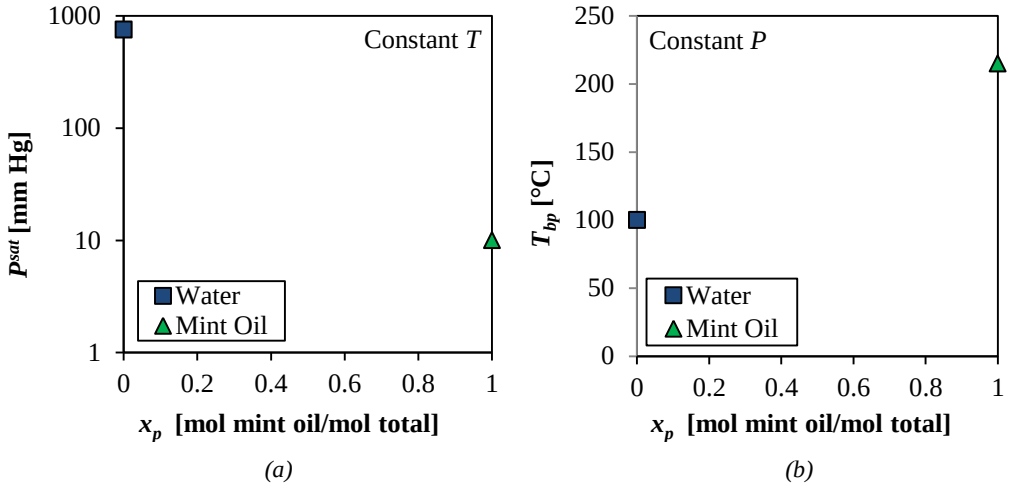

Figure 2.2.2: *Peppermint Oil and Water Binary Phase Diagrams*
(a) Saturated vapor pressure (P^{sat}) of water and peppermint oil versus peppermint oil mole fraction at constant temperature. *(b)* Bubble point temperature (T_{bp}) of water and peppermint oil versus peppermint oil mole fraction. Peppermint oil mole fraction (x_p) is known to be <0.01, therefore the saturated vapor pressure and bubble point of the binary mixture is assumed to be approximately that of water.

Energy and Water Usage:

Energy costs related to extraction of peppermint oil were estimated to be around 1.26 [$/lb oil] in 2007.[19] The peppermint oil is sold for 25 [$/lb].[20] There is potential profit to be made from peppermint farming, but other costs must be considered; e.g. labor, farm equipment fuel and maintenance, insurance, and property taxes.[20]

Distillation, as shown in the conceptual schematic in Figure 2.2.3, typically has the greatest energy usage and carbon footprint.

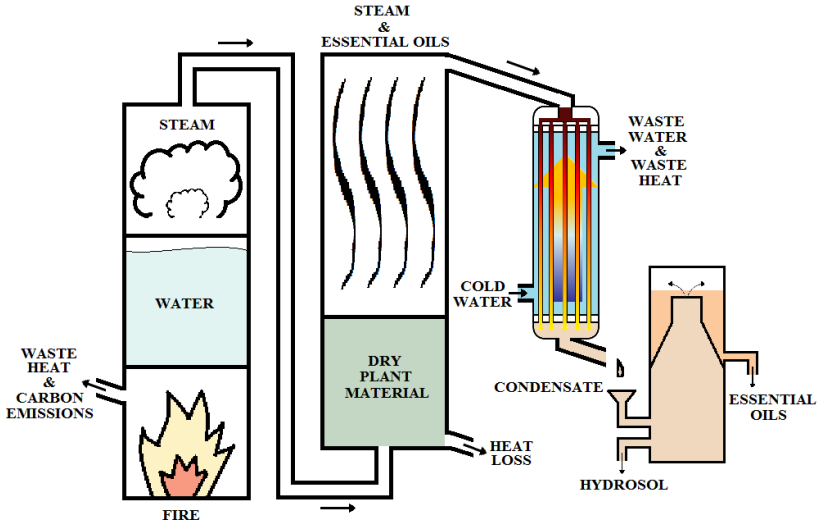

Figure 2.2.3: *Steam Distillation Schematic*
Conceptual schematic of the batch steam distillation process for the extraction of peppermint oil. A boiler is fired by fossil fuels to create steam. The steam travels through a packed bed of mint hay. The peppermint oil is transported with the steam to a tube and shell condenser. The condensate is sent to a teepee receiving can. Notice that there are several energy loss mechanisms and waste streams in this process.

Several energy waste streams shown in Figure 2.2.3 and fossil fuel consumption in the distillation process have led to increased interest in an alternative distillation technique (discussed further in Section 2.3).

Most boilers, steam pipelines, and mint tubs are not insulated; therefore exposure to heat from steam over time creates an energy inefficient process. Undesirable characteristics of the steam distillation process include chemically treated boiler water use, energy deficiencies, water waste, and carbon emissions. Energy losses due to convection and radiation around the pipelines and boilers could be significantly reduced by installing foam insulation around the steel pipes and tanks; leading to significant energy cost reductions.[19]

In addition to the energy deficiency present in steam production and transportation, the heat exchanger cooling water comes directly from a well or city water. This water exits the heat exchanger at an elevated temperature and must be cooled before recirculation.

Some farmers cool the water in a retention pond for several days before sending it to a water treatment facility. Ambient temperatures during the late-August harvest season lead to insufficient convective heat transfer and evaporative cooling due to the limited driving force for energy transfer. Reducing water usage is extremely important to the long term feasibility of mint farming and extraction practices. For example, heat from the cooling water could be used to preheat the boiler feed water.[2]

One mint trailer requires around 100 boiler horsepower [BHP] of steam for extraction. One BHP is equal to 9810 [W] of energy, where one mechanical horsepower is equal to 745 [W]. Boiler horsepower was developed because it is the amount of energy required to vaporize 30 [lbs] of 100 [°F] feed water into saturated steam at 70 [psig] in 1 [hr].[21] Steam used for oil extraction is typically created from a combination of several boilers, a total of around 1200 [BHP]. This steam is transported to different bays (6 to 12) where each mint trailer connects to the steam pipeline. Processing time is approximately 120 [min] for each trailer to breakthrough and be "exhausted" of the available mint oil. Breakthrough is defined as the amount of time for the first visible steam to exit the top of the trailer; usually around 30 [min]. The exit port at the top of the trailer is closed after breakthrough to ensure rapid transport of the steam to the condenser.

The economics of the current distillation practice are also important to consider. According to an economic study of mint farming, the installation of a mint operation on an existing farm with most equipment already available (apart from the still) would cost around 2600 [$/acre].[20] This price accounts for cultivation (water, fertilizer, and insecticide), equipment, land, insurance, taxes, and labor costs. According to that study, distillation only accounts for 15% of the total cost per acre.[20] It is unclear if this estimate includes fuel costs and annual boiler inspection and reconditioning.

Most farmers use natural gas for combustion in their boilers; with some opting for a mixture of natural gas and diesel. The use of these fossil fuels as the main energy source for combustion is a major concern when considering the long-term financial viability outlook on peppermint oil production and its carbon footprint.

The average cost of natural gas and diesel in the United States is shown in Figure 2.2.4.

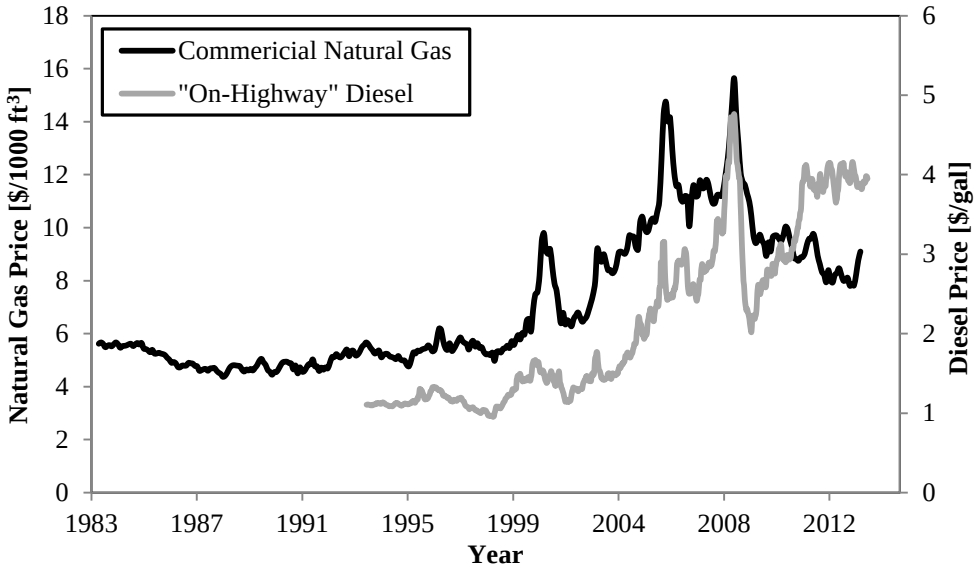

Figure 2.2.4: *U.S. Natural Gas and Diesel Price, per volume (1983 - Present)* (▬) Natural gas (NG) price for commercial consumers in dollars per thousand cubic feet (primary axis) as a function of time in the United States since 1983. (▬) "On-Highway" diesel price in dollars per gallon (secondary axis) as a function of time in the United States since 1994. Prices began to significantly increase in 1999 for both NG and diesel. Spike increases in price were seen in 2001, 2005, and 2008 for NG. Similar spikes in price occurred for diesel in 2005 and 2008. NG prices have decreased in recent years while diesel prices have continued to increase. Diesel pricing data was not available earlier than 1993. All data provided by the United States Energy Information Administration.[22,23]

A more direct comparison of these fuel costs requires analysis of the heating value (or energy density) of each fuel. High heating value is defined as the amount of heat produced by complete combustion of a given amount of material at a specified temperature.[24] Low heating values do not include the latent heat of vaporization and are typically used in boiler calculations.

The lower heating values and densities of natural gas and diesel are shown in Table 2.2.1.

Table 2.2.1: *Density and Low Heating Value (LHV) of Boiler Fuel*
Low heating value (LHV) in gigajoules (GJ), shown in terms of both mass (kg) and volume (L). The LHV per mass of NG and diesel are very similar but they differ by 3 orders of magnitude when considered on a volume basis. The density of each fuel is considered at standard temperature (T ~ 25 [°C]) and atmospheric pressure.[24]

Fuel	*Density [kg/L]*	*LHV [GJ/kg]*	*LHV [GJ/L]*
Natural Gas	7.8×10^{-4}	4.7×10^{4}	3.7×10^{1}
Diesel	8.4×10^{-1}	4.3×10^{4}	3.6×10^{4}

Accounting for the lower heating value, the cost of each fuel on an energy basis over time is shown in Figure 2.2.5.

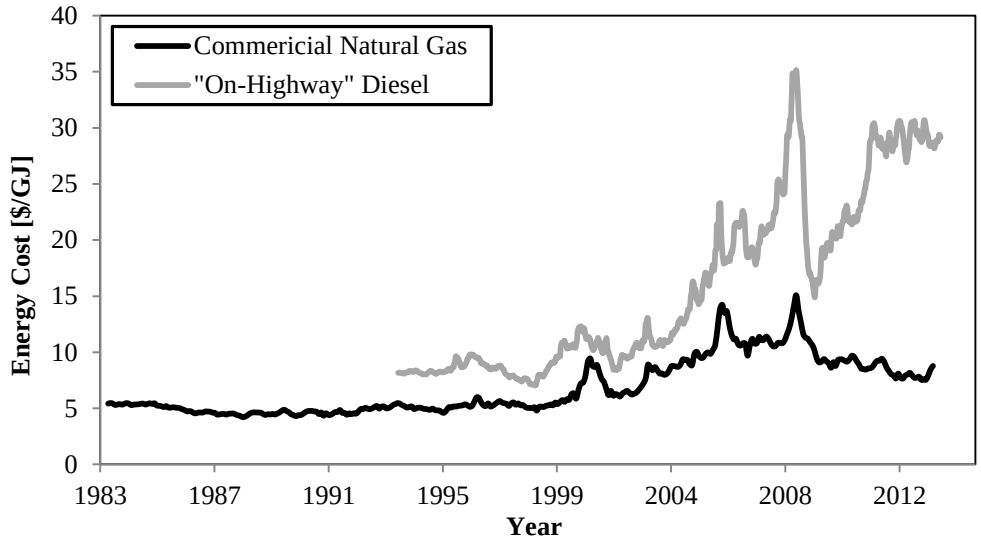

Figure 2.2.5: *U.S. Natural Gas and Diesel Price, per energy (1983 – Present)*
(▬) Natural gas (NG) price for commercial consumers in dollars per GJ of energy as a function of time in the United States since 1983. (▬) "On-Highway" diesel price in dollars per GJ as a function of time in the United States since 1994. According to the available data, diesel has always remained more expensive than NG per unit of energy. The greatest hysteresis between NG and diesel prices has been present since 2009. Currently, NG would be much cheaper than diesel to use as boiler fuel.[22,23,24]

There is no reasonable way to completely eliminate the use of fossil fuels in the cultivation of peppermint and thus elimination of carbon emissions is extremely difficult. A carbon footprint study conducted by the Mint Industry Research Council in 2009 on six U.S. mint farms provides valuable insight into the impact mint farming has on the environment.[25] That study uses carbon dioxide equivalent (CO_2e) in [kg] as the metric for

the global warming potential (GWP) of all greenhouse gases.[26] Carbon dioxide equivalent is defined by Equation 2.2.9:[26]

$$CO_2e\ [kg] = mass\ of\ gas\ [kg] * GWP\ of\ gas \qquad (2.2.9)$$

The carbon footprint was determined as a function of acres farmed and mint oil production. Four production aspects of the farming process were considered:

i. fuel used in peppermint cultivation

ii. fuel used in distillation

iii. application of inorganic fertilizer

iv. electricity use (lights, equipment, etc.)

Relative CO_2e from four different aspects of mint farming and the carbon footprint of each farm per acre of mint is shown in Figure 2.2.6.

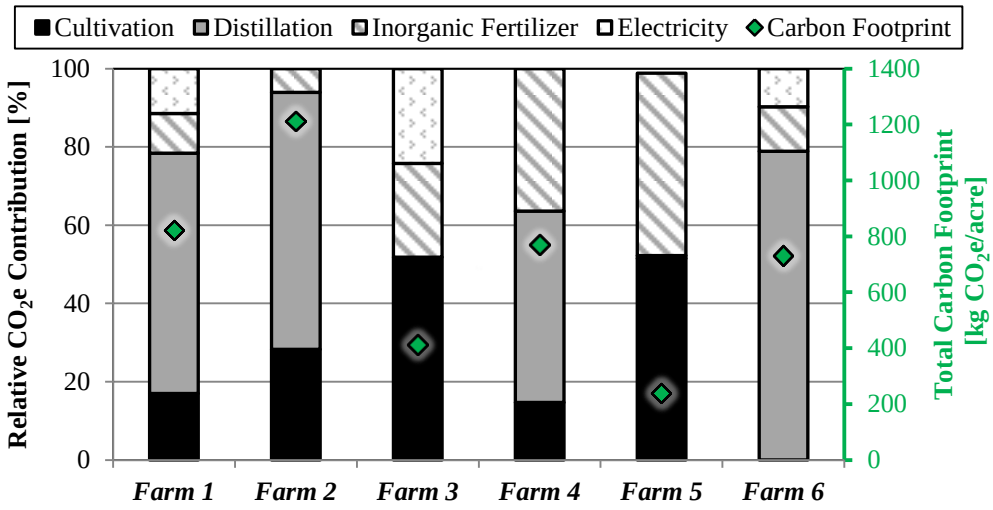

Figure 2.2.6: *CO_2e Contribution of Processes in Mint Farming* (*Primary Axis*) Relative carbon footprint contribution of fuels used in peppermint cultivation, distillation, use of inorganic fertilizer, and electricity in mint farming for six different mint farms. Farms 3 and 5 did not provide distillation data, however it can be noted that distillation is the greatest contributor to carbon emission. (*Secondary Axis*) Carbon footprint of six U.S. farms normalized for acres of mint farmed. Similar relationship observed when normalized for pounds of mint oil produced. Farms that produced more mint oil had a greater environmental impact. Data was compiled from a survey sent to several farms.[25]

Carbon footprint reduction is extremely important to companies like Wrigley's and Colgate. These companies want to market their products as "green" and sustainable.

Figure 2.2.6 shows that cultivating mint uses significant amounts of fossil fuels, which is difficult to change because most farming equipment requires gasoline or diesel fuel. The carbon footprint of the cultivation process could potentially be reduced if biodiesel were used to fuel farming equipment.

2.3. Solvent-free Microwave Extraction

Fossil fuel consumption, energy inefficiency, and the carbon footprint of traditional essential oil extraction have led to increased research and development of renewable processes and techniques. A promising alternative to traditional steam distillation is solvent-free microwave extraction (SFME). Lucchesi *et al.* have shown that essential oils obtained from basil, thyme, and peppermint oil via SFME have higher quality and contain more desirable chemical constituents than traditional steam distilled oils extracted from the same plant material.[4]

Microwaves are in a specific wavelength range of the electromagnetic spectrum and consist of alternating electronic and magnetic waves. The alternating electronic waves cause polar water molecules in the plant to rotate, increasing kinetic energy, and ultimately temperature. SFME utilizes plant material moisture as the steam source for extraction. Water vaporizes into saturated steam along with the essential oil in accordance with Raoult's Law. The subcuticular oil storage cavities are destroyed when the oil absorbs the microwave energy, rapidly expands, and causes collapse/separation of the lipid bilayer around the oil.[4]

Collapse of the oil sac increases mass transfer area of oil and enables rapid development of a saturated vapor. The microwave extraction process ruptures the oil sacs. The binary vapor mixture is then condensed and separated, similar to traditional steam distillation.

Scanning electron microscope (SEM) images of the underside of a peppermint leaf before and after extraction are shown in Figure 2.3.1.

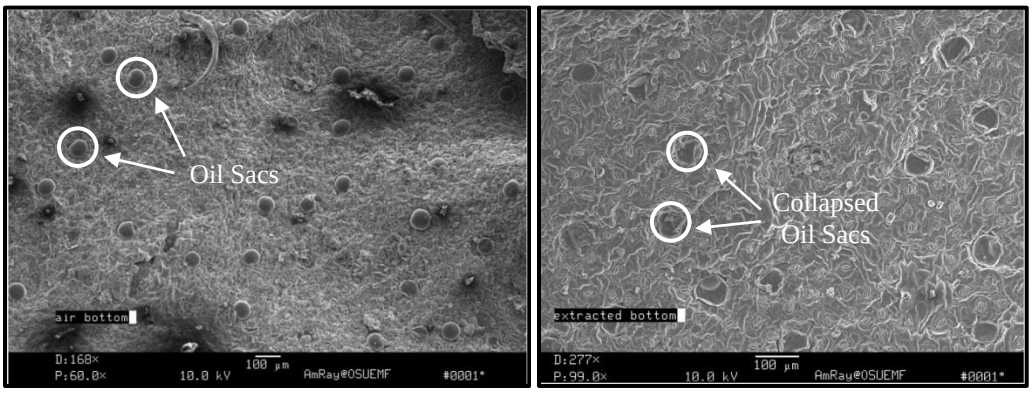

(a) *(b)*

Figure 2.3.1: *Peppermint Leaf SEM Images*
(a) Scanning electron microscope image of the underside of a peppermint leaf prior to microwave extraction. All oil sacs are intact and viable. *(b)* Scanning electron microscope image of the underside of a peppermint leaf after microwave extraction. All oil sacs are destroyed by the extraction of the oil.[19] The post-extraction image is under more magnification than the pre-extraction image.

Residential microwaves with a modified distillation unit were used as the proof-of-concept for solvent-free microwave extraction of peppermint oil.[19] The residential microwave process is a batch process, similar to traditional steam distillation. A continuous process would be superior to current batch distillation because mint still operators would have the ability to change process conditions and receive instantaneous feedback. Industrial microwaves equipped with polyethylene conveyor belts provide the opportunity for a continuous extraction process.[27]

The continuous microwave extraction process introduces a noncondensible gas (air) into the system, which causes difficulties in condensation. Condenser design is discussed in Section 2.4.

A conceptual schematic of the SFME process is shown in Figure 2.3.2. A process flow diagram for the SFME process is shown in Figure 2.3.3.

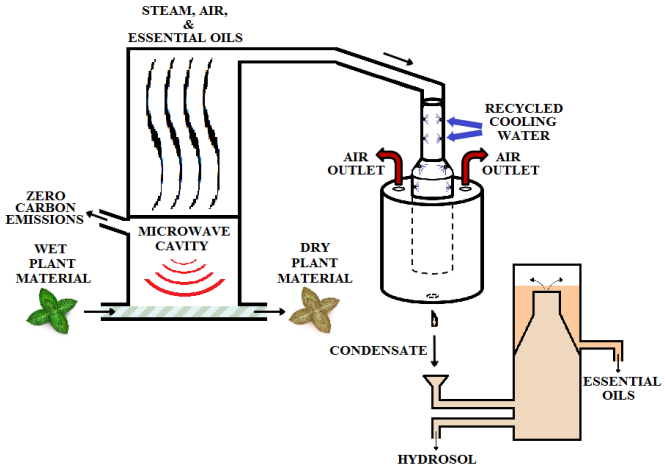

Figure 2.3.2: *Solvent-Free Microwave Extraction*
Continuous SFME process for peppermint oil extraction. Wet, unchopped plant material is fed into a microwave cavity. Steam is created from water entrapped in the plants. The peppermint oil is transported with steam to a condenser. The condenser pictured is discussed further in Section 2.4. Condensate is sent to a conical shaped separator. This process could decrease the carbon footprint of peppermint oil extraction if green or renewable energy sources provide the electrical energy for the microwave.

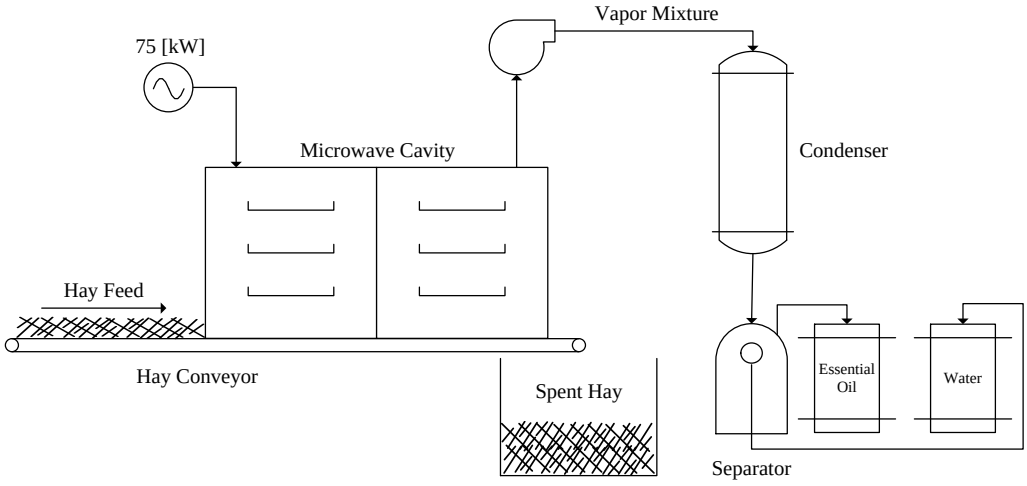

Figure 2.3.3: *Solvent-Free Microwave Extraction Process Flow Diagram*
The full process flow diagram for peppermint oil steam distillation. Peppermint plant material (hay) is fed onto a conveyor belt entering the microwave cavity. The oil and water are vaporized and transported to a condenser via a variable frequency drive (VFD) equipped blower. The condensate components are then separated in a conical shaped separator.

The most desirable chemical components in peppermint oil are menthol and menthone (Figure 2.3.4).

(a) *(b)*

Figure 2.3.4: *Important Chemical Components in Peppermint Essential Oil*
(a) Menthol is the chemical component in peppermint essential oil that gives it a distinct cooling property and "minty" taste. (b) Menthone has a carbonyl in place of the secondary alcohol in menthol. This carbonyl appears due to oxidation of the menthol molecule. The presence of menthone in peppermint oil alters the taste and properties of the oil in an undesirable way; therefore farmers make concentrated efforts to reduce menthone concentration.

Velasco *et al.* have shown that SFME produces higher quality peppermint oil with more desirable chemical components than traditional steam distilled oils. Gas chromatography (GC) was used to determine the chemical composition of essential oils. GC analysis of peppermint oil obtained in the first pilot scale SFME test in Oregon from 2009 is shown in Figure 2.3.5.[6]

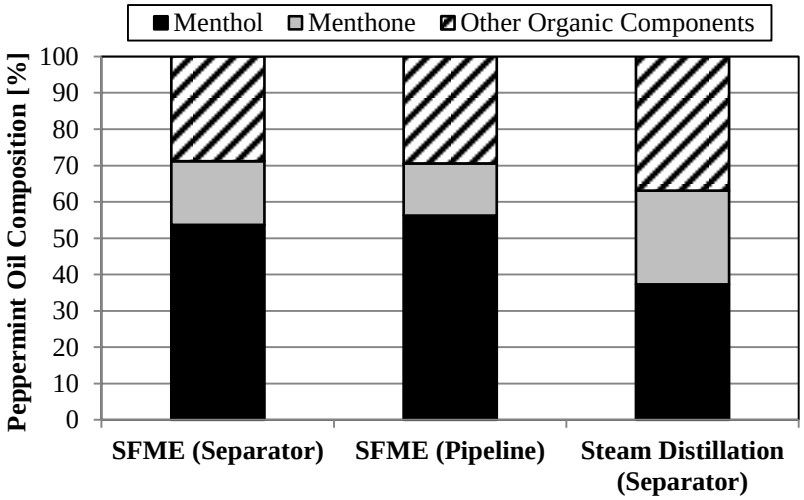

Figure 2.3.5: *Peppermint Oil GC Analysis - Stayton, Oregon Pilot Scale Test*
GC analysis of important organic components in the oil extracted at Butler Farms in Stayton, Oregon at a pilot scale test in 2009. The desired component, menthol, composes a greater portion of the overall oil in the SFME system than that of traditional steam distillation. Both oils were obtained from the same peppermint plant material. There were two locations in the SFME system where oil was located; the separator and in the pipeline from the microwave to the condenser.[6]

The molecules are less likely to be oxidized during SFME and create undesired components because the energy is applied evenly to the plant material. This explains the greater fraction of menthol present in the SFME process shown in Figure 2.3.5. Peppermint oil was found in two separate locations during the pilot scale test in 2009; in the separator unit and in the pipeline from the microwave to the condenser. This was not expected, and will be discussed further in Section 2.4.

SFME is also a valuable technique for everyday applications. A recent business venture between Dr. Hackleman and Oregon State University, OilExTech^{TM} LCC, has commercialized a home microwave distillation unit for essential oils. Consumers use plants like lavender and basil to obtain essential oil in less than fifteen minutes. The extraction device is shown in Figure 2.3.6.[28]

Figure 2.3.6: *Essential Oil Extraction Device from OilExTech^{TM} LCC*
Plant material is loaded into the glass container around the condensate cup. An ice core attached to the lid condenses the steam and oil vapors which drip down into the condensate cup. A typical extraction takes around 10 minutes from start to finish.[28]

Capital cost of an industrial-scale microwave extraction system and condensation challenges related to the presence of a noncondensable gas are possible issues for implementation. Installation of a new industrial size SFME system at an Oregon mint distillery would be very expensive. Industrial 100 [kW] microwave drying units cost approximately $200,000 for all system components and instrumentation.[27]

The microwave process reduces costs by obviating chopping. Mint is currently cut from the ground and dried for up to 2 days. Tractor choppers are then used to grind up the mint

into a finer consistency for distillation.[2] The evaporation of precious mint oil during the drying process decreases the overall oil yield. A chopper would not need to be purchased or require annual maintenance. The peppermint could be cut and immediately transported to the still for extraction. Elimination of the drying step reduces the likelihood that weather conditions could destroy the crop. Wet mint can be harvested in any weather and processed directly after it is cut.

Most of the other existing equipment and pipelines could be used for the SFME process with little modification. The spent hay from the microwave process could also be used as mulch or hay for other farming operations. Spent hay from steam distillation is extremely wet, heavy, and difficult to manage.[2] Dry mint hay mulch could be marketable as a product similar to peat moss, or as a natural herbicide/insecticide due to mint oil residues.

2.4. Condenser Design

Promising results from the Butler Farms field trial were crucial to the development of a new condensation technique.[6] The oil found in the pipeline between the microwave and the condenser was assumed to have condensed before it reached the condenser. The overall oil yield was considered low for the SFME tests when compared to the traditional steam distillation process, even though the SFME process produced more menthol. The condenser used for the field trial in 2009 was a traditional tube and shell heat exchanger, identical to those used in mint distilleries across the U.S.

Tube and shell heat exchangers are efficient at transferring heat by conduction and convection from a hot vapor to a cold fluid. The heat transfer characteristics of tube and shell heat exchangers can be described by a few simple relationships. Equation 2.4.1 is the sensible heat.

$$\dot{q} = \dot{m} C_p \Delta T \tag{2.4.1}$$

Where $\dot{q}$ is the heat transfer rate, $\dot{m}$ is fluid mass flow, C_p is fluid heat capacity, and ΔT is the temperature difference between the in and out streams.[29]. The latent heat is described by Equation 2.4.2.

$$\dot{q} = \dot{m} \Delta H_{vap} \tag{2.4.2}$$

Where ΔH_{vap} is the enthalpy of vaporization.[17] Heat exchanger performance is described by Equation 2.4.3.

$$\dot{q} = AU\Delta T_{lm} \tag{2.4.3}$$

Where *A* is the area normal to the direction of heat flow, *U* is the overall heat transfer coefficient, and ΔT_{lm} is the log mean temperature difference.[29] Equation 2.4.3 elucidates the importance of surface area to the efficacy of heat transfer in a tube and shell heat exchanger. Heat transfer rate decreases rapidly if the surface area is decreased or affected in any way. The available heat transfer area in traditional tube and shell heat exchangers is the metal surface on the tube inside walls. Cooling water typically flows in a counter-current configuration around the tubes in a shell.

Heat is transferred from the hot steam to the cold water by conduction and convection (Figure 2.4.1).

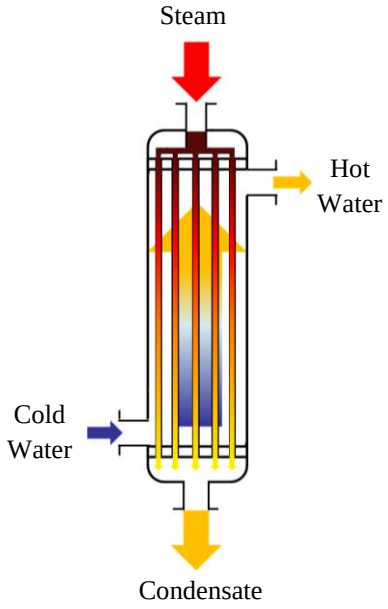

Figure 2.4.1: *Tube and Shell Heat Exchanger Schematic*
This schematic is a depiction of a typical heat exchanger used in the traditional peppermint oil distillation process. Hot vapor (Red) enters the tubes, countercurrent to the cooling water (Blue). Cooling water temperature is increased due to the heat released by steam condensation.

SFME introduces air, while traditional steam distillation is a batch process closed to the atmosphere. Continuous microwave systems have open ends at the entrance and exit to the microwave cavity allowing air to enter into the vapor mixture. Tube and shell heat

exchanger efficiency rapidly decreases with increasing air by-mass ratios.[8] The heat present within the steam is insulated by air and does not transfer through the condenser tube walls to the cooling water.

Fluid flowing past a surface, like the tube walls in a heat exchanger, transfers heat by conduction and convection.[29] The Nusselt number, *Nu*, is a dimensionless parameter used to represent the ratio of convective and conductive resistance to heat transfer (Equation 2.4.4).

$$Nu = \frac{hL}{k} \tag{2.4.4}$$

Where *h* is the convective heat transfer coefficient, *L* is characteristic length, and *k* is the fluid thermal conductivity. The Nusselt number is determined using correlations involving flow characteristics and fluid physical properties. Convective heat transfer coefficients are then determined from the Nusselt number. Air is thermally insulating, with thermal conductivity values ranging from 0.025 - 0.034 [W/(m*K)] at normal operating temperatures (0-120 [°C]).[29] The characteristic length is the tube diameter. Strong resistance to convective heat transfer could explain the undesired results seen by Hackleman *et al.* in 2009 with barely any peppermint oil in the separator.

It is proposed that when microwave radiation causes water to vaporize and create steam, the steam contacts the air and creates an aerosol, as depicted in Figure 2.4.2.[30]

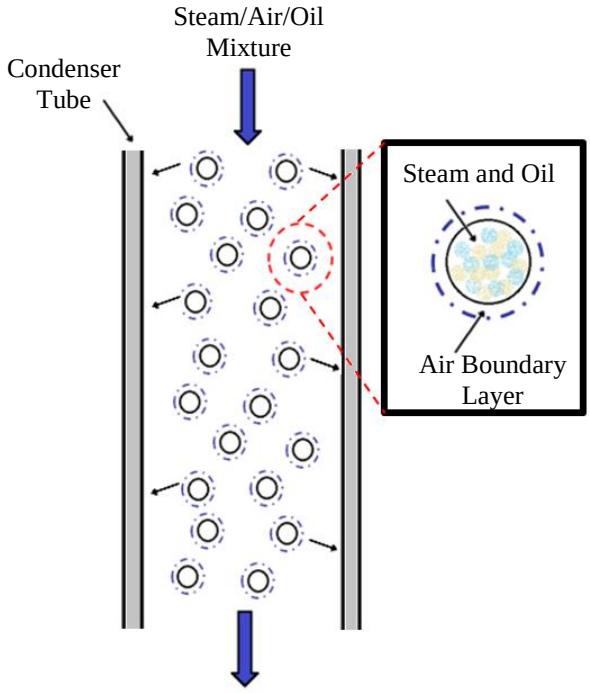

Figure 2.4.2: *Schematic of Aerosol Inside Condenser Tube*
Depiction of the steam and oil aerosol created from the SFME process. Air creates an insulating boundary layer between the vapor and condenser tube walls, decreasing heat transfer from the hot steam to the cold cooling water. Aerosols are on the order of 10 [μm].[30]

A spray scrubber-type condenser design was initially implemented in a field test conducted in North Carolina to increase heat transfer surface area.[7] The implementation of the new condenser led to increased capture efficiency of essential oil relative to the Stayton field test. The positive results seen in NC spawned a senior undergraduate chemical engineering project at Oregon State University. That team was tasked with comparing the spray scrubber condenser from NC and a traditional tube and shell condenser for the SFME process.[30]

As shown in Figure 2.4.3 a trash can, plastic nozzles, and PVC pipe were used for the initial prototype design.

Figure 2.4.3: *Condenser Prototype used by Pommerenck et al.*
Studies were conducted using a steam generation hood in a laboratory setting. Effective heat transfer coefficients and mass transfer rates were determined for different steam compositions in air.[30]

Lebsack expanded on the work of Pommerenck *et al.* and improved on the spray scrubber design and materials to create a direct-contact condenser (DCC).[8] Direct-contact heat transfer involves two fluids exchanging energy without a separating medium, like the walls of a stainless steel heat exchanger.[31] The direct-contact process also includes mass transfer between the two fluids, which can be advantageous or disadvantageous depending on the process application. Direct-contact heat transfer typically finds application in processes where high thermal energy transfer efficiency is required and mixing of streams is not an issue. For example: chemical degassers (scrubber-type) or nuclear reactor core emergency cooling systems.[32]

The DCC was fabricated and designed to withstand the harsh conditions of corrosive mint oil and increased temperatures present in the SFME process.

The DCC is shown in Figure 2.4.4.

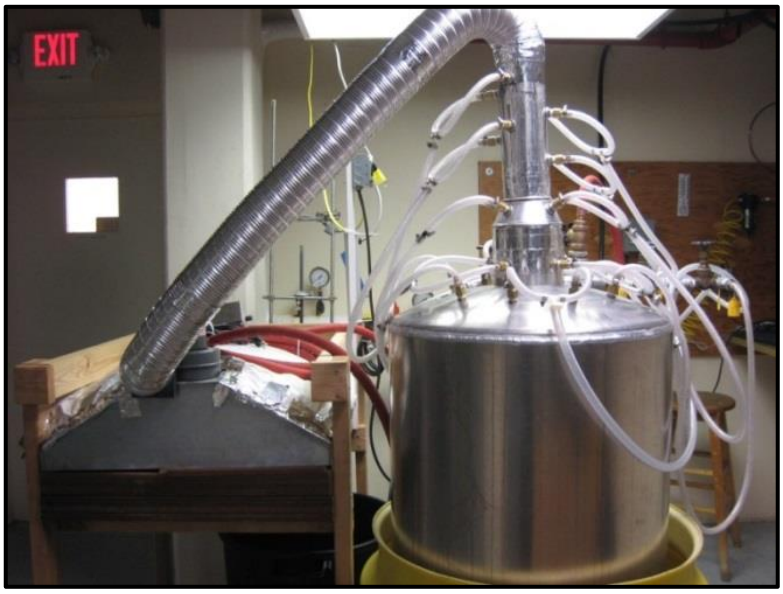

Figure 2.4.4: *Direct-Contact Condenser (DCC)*
The direct-contact condenser built and tested by Lebsack.[8] Steam generation hood (left) used to distribute steam to the condenser. Condenser (right) constructed with aluminum, stainless steel, and brass components. High temperature reinforced tubing was used because of elevated cooling water temperatures.

The DCC was tested at various steam to air mass ratios (specific humidity) and shown to be much more effective at condensing the steam-air aerosol than the tube and shell condenser.[8,30] The metric used to determine the effectiveness of each heat exchanger was recovery efficiency. Condenser recovery efficiency, η, is defined in Equation 2.4.5.

$$\eta = \frac{m_{condensate}}{m_{steam}} \tag{2.4.5}$$

Where $m_{condensate}$ is condensate mass and m_{steam} is the mass of throughout an entire experimental trial. The specific humidity, Y_w, is defined in Equation 2.4.6.[5]

$$Y_w = \frac{m_{steam}}{m_{air} + m_{steam}} = \frac{m_{steam}}{m_{vapor,total}} \tag{2.4.6}$$

Where m_{steam} is steam mass, m_{air} is noncondensible gas mass, and $m_{vapor,total}$ is total vapor mass of steam and air. The recovery efficiency is plotted against the specific humidity for different masses of steam in air.

Lebsack and Pommerenck's recovery efficiency results are shown in Figure 2.4.5.

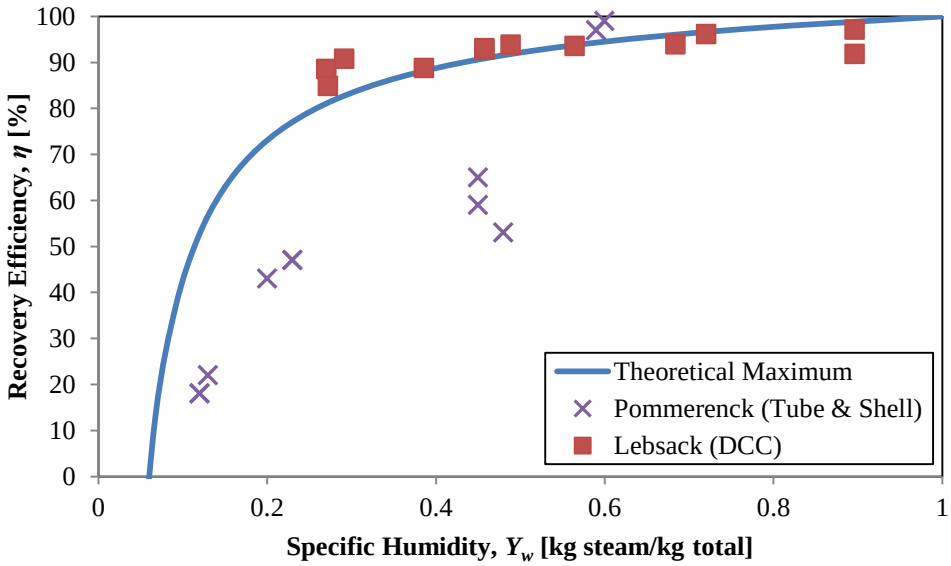

Figure 2.4.5: *Recovery Efficiency of the DCC*
The direct-contact condenser proved to be much more efficient at capturing steam at lower specific humidities (~0.3-0.6) than the tube and shell condenser. The DCC was not tested at the lowest specific humidities (< 0.25).[8,30]

The DCC outperforms the tube and shell condenser at lower specific humidity (0.3-0.6). The DCC was not fully characterized for low steam ratios ($Y_w \leq 0.25$). The theoretical maximum curve in Figure 2.4.5 was determined via an Aspen HYSYS model using the Peng-Robinson equation of state (EOS) for multiple component mixtures. The Peng-Robinson EOS accounts for repulsive and attractive interactions of the molecules much like the simpler van der Waals EOS. The Aspen HYSYS model involved mixing ambient air (20 [°C]) with saturated steam (100 [°C]) at differing mass ratios. The Peng-Robinson EOS is defined in Equation 2.4.7:[17]

$$P = \frac{RT}{(v-b)} - \frac{a \cdot \alpha(T)}{v(v+b)+b(v-b)}, \tag{2.4.7}$$

where

$$a = 0.45724 \frac{R^2 T_c^2}{P_c}, \tag{2.4.8}$$

$$b = 0.07780\frac{RT_c}{P_c}, \tag{2.4.9}$$

$$\alpha(T) = \left[1 + \kappa\left(1 - \sqrt{T_r}\right)\right]^2, \tag{2.4.10}$$

$$\kappa = 0.37464 + 1.54226\omega - 0.26992\omega^2, \tag{2.4.11}$$

where P is system pressure, R is the ideal gas constant, T is system temperature, v is molar volume, T_c is critical temperature, P_c is critical pressure, T_r is reduced temperature (T/T_c), and ω is the acentric (non-sphericity) factor. Each value is specific to either air or steam.

3. Materials

3.1. Microwave Unit

At the Cellencor™ Inc. facilities in Nevada, Iowa, a 75 [kW] AMTek Microwaves test system was utilized.[33,27] Applied microwave power was adjustable from 0 to 75 [kW]. The microwave generator has 90% electrical conversion efficiency and 80% total system efficiency. The system is equipped with a 500 [gal] water cooling tank to cool the microwave generator. The microwave operates at a typical commercial frequency of 915 [MHz], where most home microwaves operate at 2.45 [GHz]. Most commercial microwave systems operate at 915 [MHz] because they are more energy efficient and less expensive to operate than 2.45 [GHz] systems.[34] The lower frequency also allows a greater physical opening at the feed entrance and exit for a given length of RF choke.[6] The system used here is capable of drying approximately 8 [tons/day] of 10-40 [%] moisture content material, removing 280 [lbs/hr] of water.[27]

The microwave cavity measured 10 x 4.33 x 4.33 [ft]. Heavy duty metal waveguides transported the microwaves into the cavity. Two open mesh polyethylene (PE) conveyor belts were used to compress and transport the mint hay through the microwave cavity. The belt speed was adjustable from 10 to 100 [in/min], with a usable width of 12 to 42 [in]. Two adjustable metal/PE guides at the conveyor belt entry provided a uniform width of plant material across the belt surface in the cross-machine direction. Hay thickness was adjusted manually by two human operators. A 115 volt, 230 [CFM] Dayton permanent split capacity blower was used to transport the vapor stream exiting the microwave to the condenser.[35] An Allen-Bradley® Powerflex® 40 AC variable frequency drive (VFD) was used to adjust the blower flow rate.[36]

The system was instrumented with input, output, and internal temperature probes. The input and output temperature sensors are direct-contact resistance temperature detectors (RTDs). RTDs measure change in metal resistivity with temperature, where thermocouples measure a voltage difference between two metals.[37] Two infrared (IR) temperature sensors were used inside of the microwave cavity, as they do not require direct contact with the material. IR sensors within the cavity and input and output RTDs were not used due to system configuration. The sensors are mounted above the conveyor

belts and are only operational when the bottom belt is the only belt in use. The microwave generator also has an Allen-Bradley PanelView 600 energy monitor to track energy usage and instantaneous power.[38] The microwave cavity is shown in Figure 3.1.1.

Figure 3.1.1: *Photograph of the Microwave Cavity*
Industrial microwave used on site in Nevada, Iowa. Shown here from the exit of the microwave cavity (left), with two doors for cleaning unit interior and fire suppression from dielectric arc.

Peppermint plant material used for testing in Iowa was donated by John Reerslev of Reerslev Farms in Junction City, Oregon, in early August, 2012. Mr. Reerslev is the Oregon state representative for the MIRC. Two types of plant material were gathered in Junction City, Oregon, and are described in Table 3.1.1.

Table 3.1.1: *Peppermint Gathered from Reerslev Farms - Junction City, OR*
Peppermint types used for experimentation in Nevada, Iowa. All plant material was gathered in early August, 2012, and stored in 20 [gal] PE bags at the Hyslop Crop Science Field Research Laboratory industrial freezer.

Plant Material	Location	Description
"Wet" Hay	Field	Freshly cut after long-term growth
"Dry" Hay	Mint Still	Cut, chopped, and dried for distillation

All plant material was stored in 20 [gal] PE bags at the Hyslop Crop Science Field Research Laboratory industrial freezer to preserve the material for later testing. The plant material was then transported in a 4 x 4 x 8 [ft] U-Haul trailer with Styrofoam™ insulated walls and dry ice for the 30 hour drive to Iowa from Corvallis, OR.[39] The bags

of mint were left in the trailer until needed for testing. Each bag was transported from the trailer to the microwave with a 100 [gal] plastic wheelbarrow provided by Cellencor™.

A spray bar was fabricated and used to increase the moisture content of the dry peppermint hay before entering the microwave cavity. The spray bar was constructed with 1/2 [in] OD PVC pipe, "garden" hose, and a TeeJet® VisiFlo® Flat Spray Tip nozzle assembly.[40] Spray bar flow rate was regulated with a ball valve and pressure gauge. The spray bar assembly is shown in Figure 3.1.2.

Figure 3.1.2: *Spray Bar Assembly*
Spray bar assembly used above conveyor belt before entry into microwave cavity. One nozzle was used to spray all plant material (left), the rest of the nozzles were plugged. Metal/PE material guides are shown resting on the bottom conveyor belt.

A Mettler - Toledo HB43-S Halogen Moisture Analyzer was used to determine hay moisture content (MC) before and after processing.[41]

3.2. Direct-Contact Condenser

A direct-contact condenser (DCC) previously described was constructed with aluminum and 316 stainless steel because of the corrosive resistance of these materials. [8] The construction and development of the condenser is thoroughly discussed by Lebsack and schematics taken from the report describing condenser dimensions can be found in Appendix A.

The assembled condenser used on site in Iowa is depicted in Figure 3.2.1.

Figure 3.2.1: *Direct-Contact Condenser in Nevada, Iowa*
DCC connected to AMTek^{TM} microwave system, the microwave, pump, and valve assembly are not shown. The yellow container is the cooling water reservoir. Not shown is the platform balance upon which the condenser assembly was placed.

The center column and condenser shell were equipped with 24 Lechler 460 series full cone spray nozzles (Model #: 460.528, 120° spray angle, 0.60 [GPM] at 40 [psi]).[42] A 1.5 [HP] high-capacity Flotec sprinkler pump was used to recycle cooling water sprayed from the DCC into the 65 [gal] reservoir.[43,44] A bypass valve was used to adjust system pressure and nozzle flow rates. Kentak clear vinyl tubing [1/4" OD, -28 to 65 $^{\circ}$C] was used to deliver recycled cooling water from the pump to the spray nozzles.[45]

Prior to experimentation in Iowa, the condenser exhaust ports were expanded in diameter from 1.5 to 3.5 [in] because of throughput concerns with the 75 [kW] microwave system. The DCC characterization previously conducted had the exhaust exited directly to the surroundings.[8] The Iowa facility required effluent air to be exhausted outside. New 4 [in] aluminum ducting connected the exhaust port on top of the microwave cavity to the condenser inlet and also connected the condenser exhaust to the existing building

exhaust. The cooling water reservoir was replenished with fresh potable water after each experimental trial using a Zoeller Model 98 Automatic Mighty Mate 1/3 [HP] Sump Pump.[46]

The DCC was instrumented with vapor input, output, and cooling water reservoir temperature probes. Vapor inlet and outlet were also equipped with relative humidity (RH) probes. An Extech AN100 CFM/CMM Mini Thermo-Anemometer was used intermittently at the steam/air exhaust.[47] Vernier® type K thermocouples and Omega® RTDs were used to gather temperature measurements from the input and outputs.[48,49] Recycled cooling water reservoir temperature was measured with a Vernier® type K thermocouple. Thermocouples were used with a LabQuest® handheld data acquisition device.[50] A Scalerite 1000 [kg] capacity platform scale was used to measure condensate mass.[51] The platform scale was tared for a given mass of cooling water before each experimental trial. The mass of condensate was assumed to be the accumulation of water over the duration of each trial. DCC process flow is depicted in Figure 3.2.2.

A PY-25 pyramid receiving can was acquired from Newhouse Manufacturing of Redmond, Oregon, for essential oil separation but not used during experimentation.[52] The top liquid layer in the DCC recycle tank was to be removed to the pyramid receiving can by a SHURflo® M8000 high pressure electric diaphragm pump (1.8 [gpm] capacity).[53] The SHURflo® volumetric flow capability was too great for the maximum allowable volumetric flow of the separator (0.8 [gpm]).

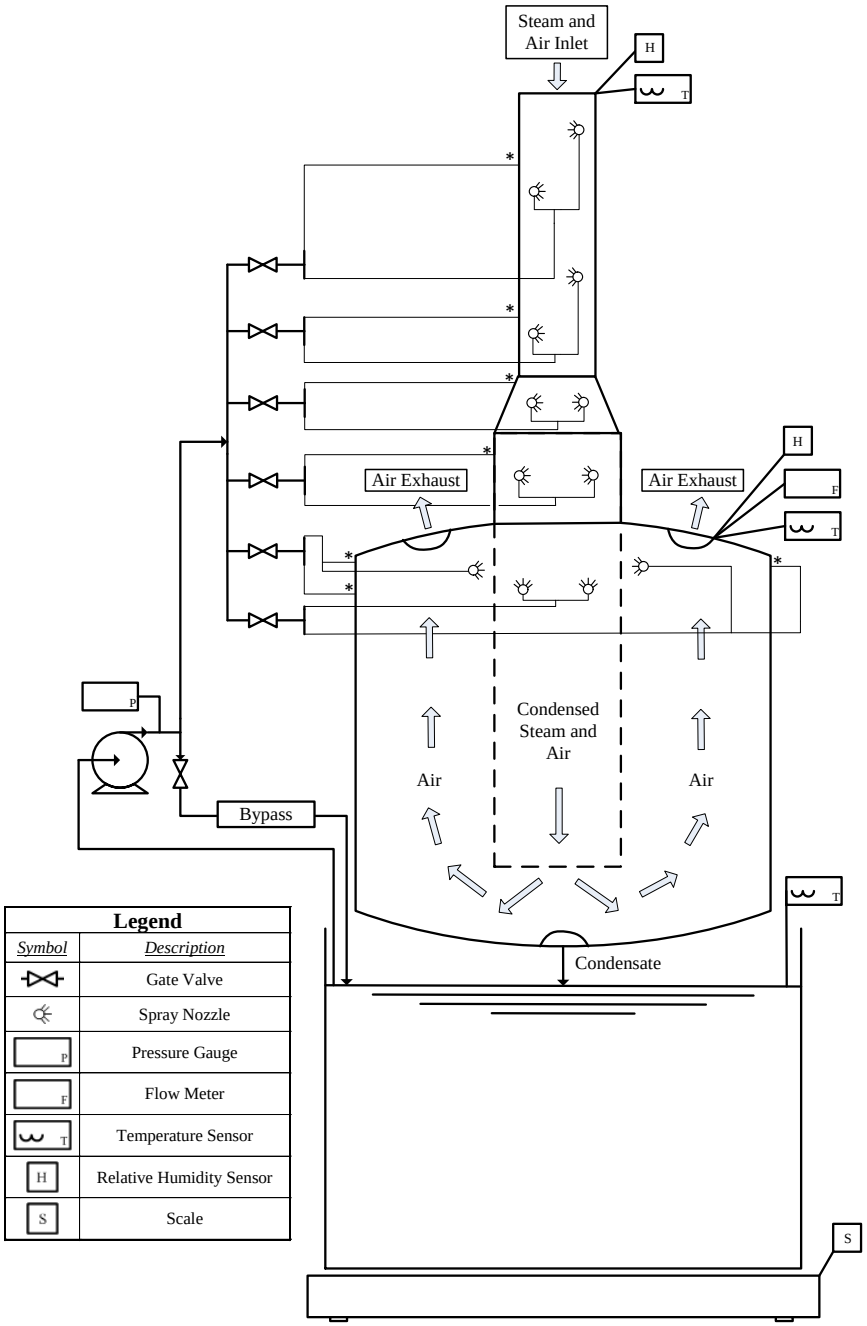

Figure 3.2.2: *Direct-Contact Condenser Process Flow*
The DCC enhanced process flow diagram shows the movement of recycled cooling water through the system including valves, nozzles, and pipelines. Twenty four nozzles are installed in the center column and condenser shell. The "*" denotes a pipeline traveling to spray nozzle(s) on the opposite side of the condenser. Vernier® type K thermocouples and Omega® RTDs measure temperature at the vapor inlet and exhaust. Reservoir temperature was measured with a Vernier® type K thermocouple. An industrial capacity scale was used to measure condensate mass.

3.3. Spray Nozzles

A single Lechler nozzle was tested to investigate droplet characteristics. The experimental setup consisted of a “garden” hose attached to house water and plumbed to a gate valve (Figure 3.3.1).

(a) *(b)*

Figure 3.3.1: *Peppermint Leaf SEM Images*
(a) Spray nozzle experimental test setup. System pressure was regulated with a gate valve. *(b)* Detail of spray nozzle test apparatus used in bench top experiments. High speed photographs of the spray were taken when system pressure was 40 [psi].

A pressure gauge was installed directly upstream of the nozzle outlet. Flow was controlled with the gate valve to achieve the desired operating pressure. High speed photographs of the spray were taken to estimate droplet size (shown in Section 5.2).

4. Methods

4.1. Experimental Design

The experiments conducted in Iowa were designed to test the feasibility of the entire continuous microwave extraction system and analyze the recovery and energy efficiencies of the DCC at condensing the incoming vapor in the presence of noncondensible air.

Equipment Set-up:

All DCC equipment and peppermint plant material were transported from Oregon to Iowa in a 4 x 4 x 8 [ft] U-Haul trailer rented in Corvallis that was modified into a makeshift refrigerated trailer with ½ [in] Styrofoam™ insulation and plastic containers filled with dry ice. The trailer maintained the integrity of the peppermint plant through the 3 day drive. The research team assembled and constructed all equipment at the Biomass Energy Conversion (BECON) test facility in Nevada, Iowa, where Cellencor™ is located. Assembly and construction of all equipment required a full work day. The DCC and associated instrumentation was positioned on the opposite side of the microwave cavity doors for safety and ease of access. Peppermint hay was transported from the refrigerated trailer to the testing area with 100 [gal] heavy-duty plastic wheelbarrows.

The experimental equipment layout is shown in Figure 4.1.1.

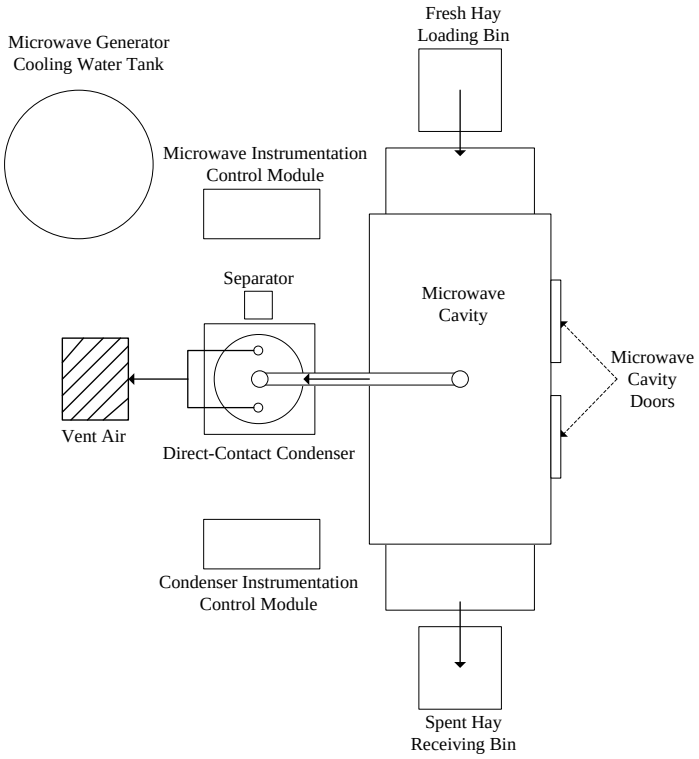

Figure 4.1.1: *Plan View of the Equipment Layout in Nevada, Iowa*
Equipment layout for experiments conducted in Iowa. The microwave cavity and all associated pieces were fixed in position. The DCC was placed on the opposite side of the microwave cavity doors to allow easy fire and cleaning access.

Start-up:

Peppermint hay material was loaded into the cavity before the microwave generator was turned on to decrease the risk of a dielectric arc. Loading the cavity prior to turning on the microwave generator provided uniform heating of the plant material. Hay was manually placed on the bottom conveyor belt at a width of 24 [in], depth of 2 [in] and belt speed of 12 [in/min]. Hay was conveyed until it was observed exiting the cavity outlet into the 100 [gal] wheelbarrow. Microwave generator power was then set to 25 [kW] and increased 10 [kW] every 2 [min] until a power of 60 [kW] was obtained.

The blower and DCC cooling water were not in operation until steam vapor was observed exiting the open ends of the microwave cavity; indicating it was saturated with steam. Blower speed was adjusted with the variable frequency drive (VFD). All trials had the

VFD set to 60 [Hz], the maximum allowable frequency for safe operation. The DCC cooling water pump was turned on after the VFD was set. Only 16 of the 24 installed cooling nozzles were used during experimental trials. The 8 nozzles in the condenser shell were known to cause uncondensed water from the spray to get entrained in the airflow, escaping through the air exhaust ports.[8] Temperature, relative humidity and moisture content of the plant material were recorded over the entire experiment duration. Trials were limited to approximately 45 [min] due to the maximum allowable temperature of the recycled cooling water (46 [°C]). Steam increases the temperature of the recycled cooling water over the duration of each experiment. As discussed in Section 2.2, the optimal separation temperature of mint oil and water is 46 [°C].

Experimental Trials:

The continuous microwave extraction process flow diagram with instrumentation is shown in Figure 4.1.2.

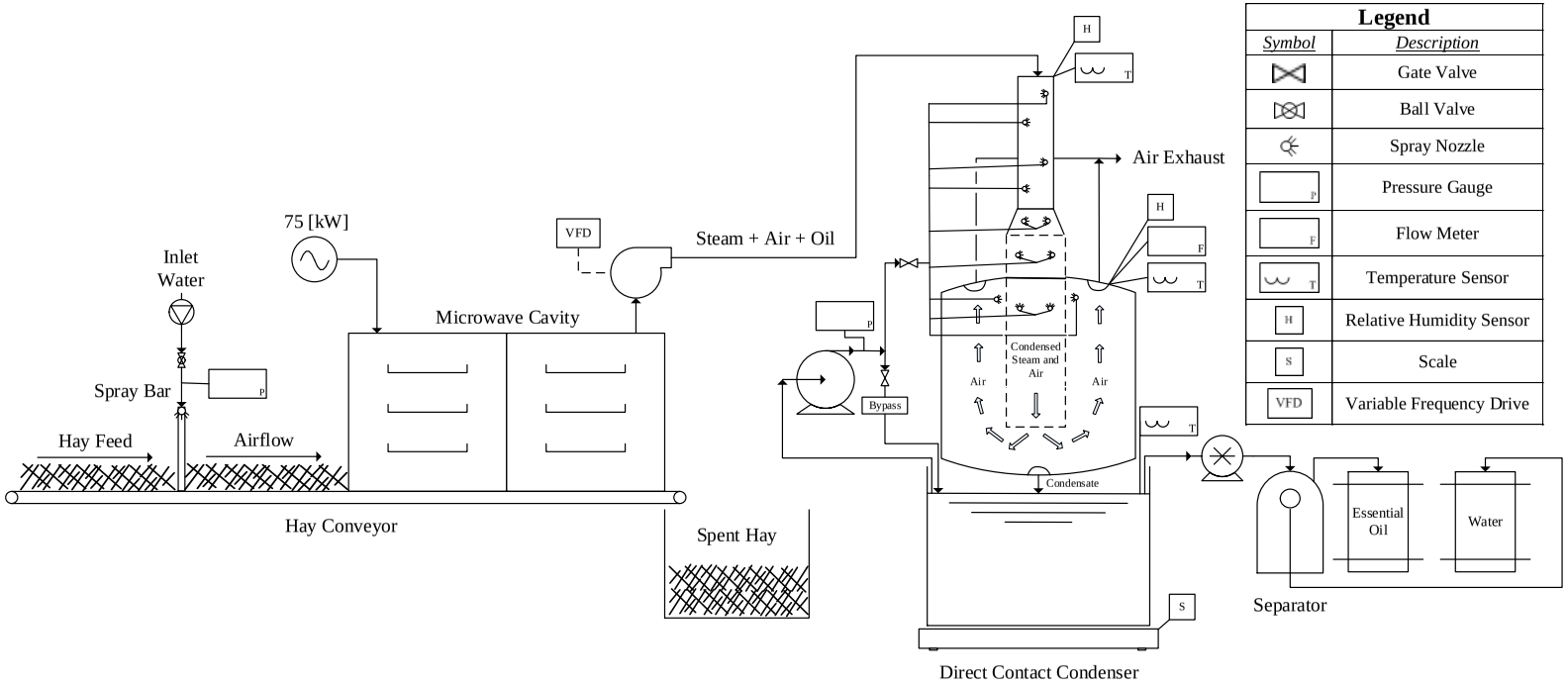

Figure 4.1.2: *Complete Microwave Process Flow Diagram*
Continuous extraction of essential oil from plants with microwave technology. Hay is fed manually onto conveyor belt. A spray bar is installed for use with dry hay. A VFD controls the blower volumetric flow to the direct-contact condenser (DCC). DCC recycles cooling water from the reservoir to spray nozzles. At the end of an experimental trial a diaphragm pump is used to transfer the top layer of water and oil to the separator. All instrumentation used is shown. It is important to note that there are several spray nozzles and corresponding pipelines NOT depicted here.

Process parameters were estimated for an ideal extraction process from previous pilot-scale microwave extraction experiments[6,7] and studies on the DCC.[8] Several of these initial parameters were changed in order to achieve a higher steady state temperature at the condenser inlet. Important process parameters were: hay throughput, hay moisture content, applied microwave power, number and location of nozzles used on condenser, nozzle flow, and initial cooling water temperature. The process parameters used for pilot scale SFME in Iowa are shown in Table 4.1.1.

Table 4.1.1: *Process Parameters for the Iowa Pilot Scale Experiment.*
The process parameters used during experimental trials conducted in Nevada, IA, with the pilot-scale continuous SFME system.

Parameter	*Description*	*Value*	*Units*
P_{MW}	Applied microwave power	60	[kW]
$\dot{m}_{spraybar}$	Spray bar mass flow	1.1	[kg/min]
W_{hay}	Hay width on conveyor	24	[in]
D_{hay}	Hay depth on conveyor	2	[in]
v_{belt}	Conveyor speed	12	[in/min]
MC_{before}	Inlet hay moisture content	35	[%]
V_{tank}	Water volume in cooling tank	30	[gal]
N	# of nozzles in use on DCC	16	[nozzles]
$T_{c,i}$	Initial cooling water temperature	17	[°C]

The conditions listed in Table 4.1.1 provided a hay throughput of approximately 1.5 [yd^3/h]. A typical mint tub trailer carries around 30 [yd^3], operating for approximately 90 [min], this gives a hay throughput of approximately 20 [yd^3/h]. Recall from Section 2.2 that each tub requires approximately 100 [BHP] for extraction, or according to Equation 4.1.1:

$$1\ [BHP] = 9810\ [W] \quad \rightarrow \quad 100\ [BHP] = 981\ [kW] \qquad (4.1.1)$$

Examination of the energy usage per cubic yard of plant material shows that the microwave process uses approximately 40 [kWh/yd^3] compared to 49 [kWh/yd^3] for the steam distillation process.

Photographs of the system on site in Iowa are depicted in Figures 4.1.3 and 4.1.4.

Figure 4.1.3: *Photograph of the DCC and Microwave Cavity*
Direct-contact condenser (DCC) and backside of the microwave cavity used for experiments in Nevada, Iowa. The blower connected to the condenser inlet was moved from the bottom of the microwave cavity (not shown) to the top of the microwave cavity (depicted here).

Figure 4.1.4: *Photograph of the Conveyor Belt and Adjustable Guides*
Microwave conveyor belt and adjustable guides for hay width. Hay pictured here was the "dry" material. The spray bar used to increase the moisture content of the hay is also pictured.

Figure 4.1.5 depicts the “wet” un-chopped peppermint plant material being loaded onto the conveyor belt.

Figure 4.1.5: *Photograph of Wet Peppermint Hay Entering the Microwave*
Wet un-choppped peppermint plant material entering the microwave cavity. Previous to the experiments conducted in Iowa, wet plant material had never been tested on a pilot-scale microwave system. Pictured on the left is Dr. David Hackleman (Oregon State) and on the right is Dr. Peter O’Daniel (IP Callison & Sons).

During experimentation, many dielectric arcs created fires inside of the cavity. Each dielectric event caused a temporary shut-down of the unit and, consequently, limited data collection. A solution was proposed by Dr. Hackleman: place a “load” into the cavity to absorb some of the microwave energy and reduce dielectric arcing. A scheme was then developed which resulted in the elimination of dielectric arcing. It is a proprietary and confidential discovery that Cellencor^{TM} now uses to resolve issues within their customer base.

4.2. Steam Material and Energy Balance

Data gathered in Iowa was analyzed in a similar fashion to that of Lebsack *et al.* in order to provide direct comparison of the results of the separate experiments with identical equipment. Steam mass flow entering the DCC from the microwave system must be determined to evaluate DCC recovery efficiency (Equation 2.4.5). Water mass flow exiting the condenser as uncondensed water vapor must first be determined. Velocity of

the vapor mixture of air and uncondensed water vapor exiting the exhaust port of the DCC was used to find the volumetric flow of the vapor mixture exiting the system (Equation 4.2.1):

$$\dot{V}_{exhaust} = v_{exit}\pi R_{exhaust}^2, \tag{4.2.1}$$

where $\dot{V}_{exhaust}$ is DCC exiting vapor volumetric flow, v_{exit} is vapor velocity, and $R_{exhaust}$ exhaust radius. Equation 4.1.1 must be multiplied by a factor of 2 to account for both DCC exhaust ports. Vapor volumetric flow is used to determine the mass flow if the density is known. Exiting vapor temperature can be used to determine the saturation vapor density using the ideal gas law (Equation 4.2.2).

$$\rho_{sat} = \frac{\dot{m}_{water}}{\dot{V}_{exhaust}} = \frac{\dot{n}_{water}M_{water}}{\dot{V}_{exhaust}} = \frac{P^{sat}M_{water}}{RT_{air}} \tag{4.2.2}$$

Where P^{sat} is saturation vapor pressure of water in air, V_{air} is air volume, $\dot{n}_{water}$ is water molar flow, M_{water} is water molecular weight, and ρ_{sat} is saturation vapor density of water in air. Saturation vapor pressure of air at different temperatures was determined using Antoine's Equation.[16]

The specific humidity must be determined in order to compare experimental data directly to Lebsack *et al.* Aspen HYSYS simulation of mixing air at 20 [°C] with steam at 100 [°C] was performed by Lebsack *et al.* to determine the estimated specific humidity at a given temperature.

The saturation vapor density of air is shown with the results of the Aspen HYSYS air and steam mixing simulation in Figure 4.2.1.

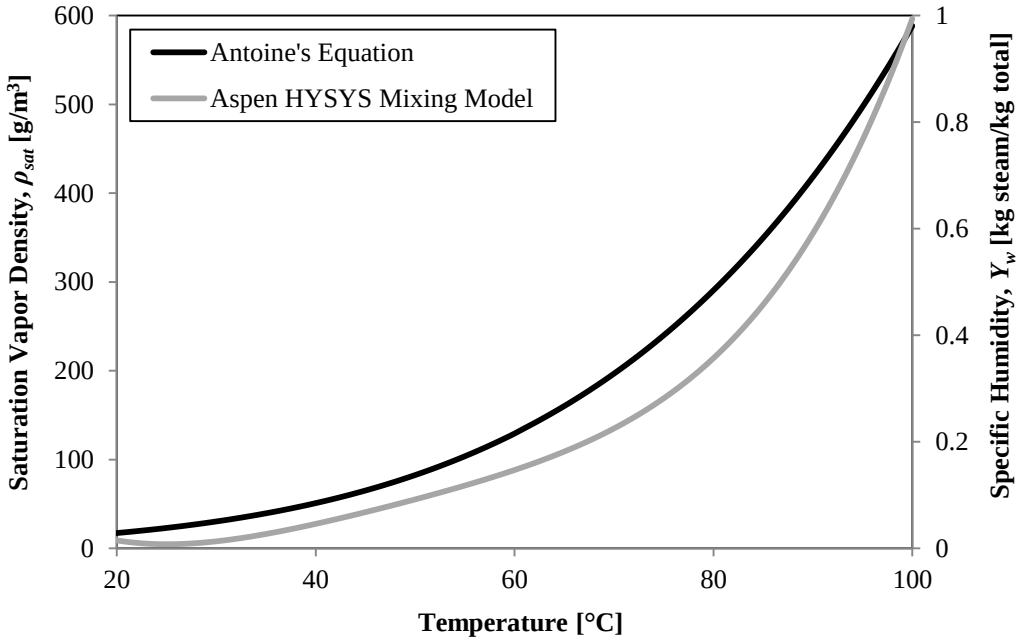

Figure 4.2.1: *Saturation Vapor Density of Air and Aspen HYSYS Specific Humidity* (*Primary axis*) Saturation vapor density of water in air over a range of temperatures. The saturation vapor density was used to determine the mass flow of steam exiting the DCC.[8] (*Secondary axis*) Specific humidity of a steam and air mixture over a range of temperatures[8] Specific humidity is used to compare condenser recovery efficiency data to that gathered by Lebsack *et al.*

Saturation vapor density of water in air is used to convert from volumetric flow to mass flow. Condenser inlet and exhaust temperatures were measured in order to determine the percent water by mass in the vapor mixture. Water mass flow exiting the system, $\dot{m}_{water,exit}$, can be determined from Equation 4.2.3.

$$\dot{m}_{water,exit} = \dot{V}_{exit}\rho_{sat,i}(T_{exit}) \tag{4.2.3}$$

Where $\rho_{sat,i}$ is a function of the temperature at the exit (T_{exit}). Due to conservation of mass, water entering the condenser as steam will either condense or exit out of the exhaust ports as vapor trapped in air. The material balance on steam is shown in Equation 4.2.4.

$$\dot{m}_{steam,in} = \dot{m}_{water,exit} + \dot{m}_{condensate} \tag{4.2.4}$$

Condensate mass flow, $\dot{m}_{condensate}$, is measured by the platform scale every minute. Steam mass flow into the DCC, $\dot{m}_{steam,in}$, is determined using an energy balance on steam. Combining Equation 2.4.1 and 2.4.2 leads to Equation 4.2.5.

$$\dot{q}_{in} = \dot{m}_{steam,in}\left(C_{p,water}(T_{in} - T_{ambient}) + \Delta H_{vap,steam}\right) \qquad (4.2.5)$$

Where $\dot{q}_{in}$ is microwave energy applied and $T_{ambient}$ is ambient air temperature. Steam mass flow can be verified by measuring plant material moisture content (MC) of entering the microwave cavity, and taking another MC measurement from a sample exiting system. The difference in MC corresponds to the maximum mass flow of water vapor into the condenser. DCC recovery efficiency is then determined via the cumulative mass of condensate and steam into the DCC for a given time interval as shown in Equation 2.4.5 (repeated below):

$$\eta = \frac{m_{condensate}}{m_{steam,in}} \qquad (2.4.5)$$

Recovery efficiency is plotted versus specific humidity and compared to a maximum theoretical efficiency. Maximum theoretical recovery efficiency was determined by assuming T_{exit} to be 46 [°C], the optimal separation temperature of peppermint oil and water, and is shown in Figure 4.2.2.

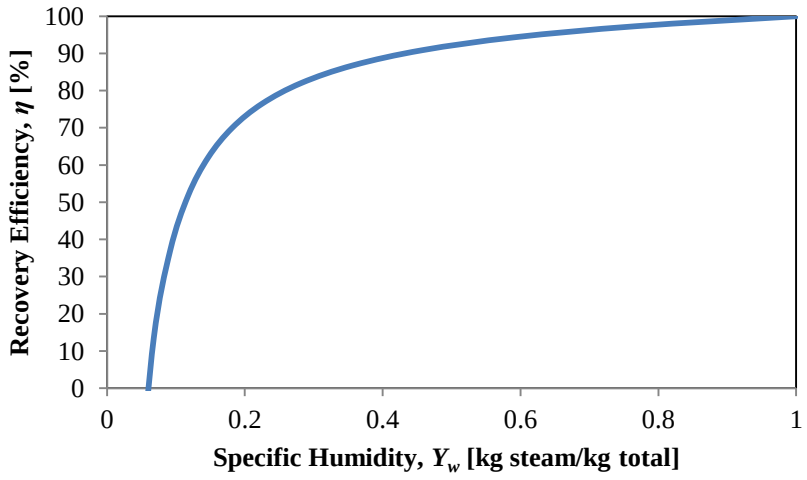

Figure 4.2.2: *Theoretical Condenser Recovery Efficiency (T_{exit} = 46 [°C])* Maximum theoretical recovery efficiency of a DCC assuming an exit temperature of 46 [°C]. The curve was extended for lower values of specific humidity, $Y_w < 0.1$, from that shown by Lebsack *et al.*[8] The DCC will not condense any steam if the specific humidity is < 0.05.

4.3. Spray Nozzle Droplet Size Determination

The spray nozzles chosen for the DCC are extremely important to the heat and mass transfer efficiency of the device. Effectiveness of the spray condenser is related to droplet size, droplet velocity, spray angle, and spray column diameter. Volume fraction of the droplets (or holdup), ϕ_d, is defined by Equation 4.3.1.[5]

$$\phi_d = \frac{V_d}{V_T} \tag{4.3.2}$$

Where V_d is dispersed phase volume (droplets) and V_T is total contacting volume within the DCC. The droplets created in the DCC were sprayed radially at different locations along the length of a 4 [in] inside diameter (ID) aluminum pipe. Spray nozzles in the DCC shell were not used for experimentation because water escaped from the exhaust ports when they were in operation. System pressure was maintained at 40 [psi] with corresponding cooling water flow of 0.60 [GPM/nozzle].

A droplet size distribution is created inside the DCC. Sauter mean diameter (SMD) is used to simplify the overall droplet size distribution. SMD is defined as "the diameter of a droplet whose volume-to-surface ratio is equal to that of the entire spray".[54] SMD is the most commonly used diameter in the spray industry due to mass and heat transfer applications. SMD (D_{32}) is defined in Equation 4.3.2:

$$D_{32} = \frac{\sum N_i D_i^3}{\sum N_i D_i^2} \tag{4.3.2}$$

where i is the size range considered, N_i is drop number, and D_i is the middle diameter of size range i. The nozzle analysis provided by Lechler showed a SMD of 261 [µm].[42] The surface area is relevant to the mass transfer of cooling water to the hot aerosol particles. Droplet size distribution information could aid in the development of an improved DCC for increased mass and heat transfer rates.

Droplet size distribution on a volume basis measured by the manufacturer was provided by Lechler Nozzles and is shown in Figure 4.3.1. Experimental conditions for this droplet size distribution were different than those used in the DCC, but still provide crucial insight into the droplet characteristics.

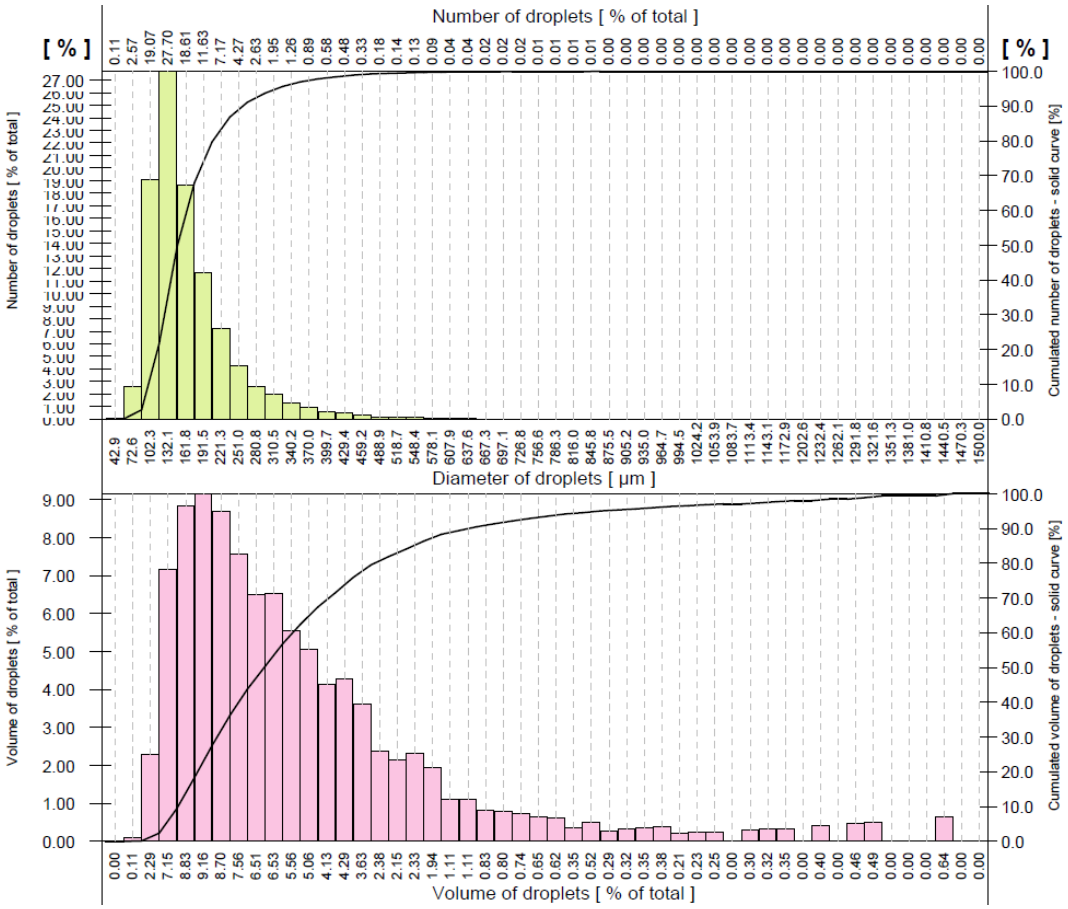

Figure 4.3.1: *Lechler 460.528 Spray Nozzle Droplet Size Analysis*
Droplet size distribution of a Lechler 460.528 spray nozzle. Measurement conditions were a pressure of 36 [psi], water flow of 2.20 [L/min] and spray distance of 8 [in]. Sauter mean diameter was 261 [µm].[42] The spray nozzles used in the DCC were operated at a pressure of 40 [psi], volumetric water flow of 2.27 [L/min], and a spray distance of 4 [in]. Greater spray distance allows droplets to break away from one another due to turbulence and leads to decreased droplet diameter. The droplet size distribution created in the DCC probably centers around diameters greater than those observed in the figure.

The SMD is used for modeling and analysis of spray extractors because it directly related to holdup and interfacial area when spherical droplets are assumed.[5]

SMD can also be expressed by Equation 4.3.3.[5]

$$D_{32} = \frac{6\varepsilon\phi_d}{A_d} \tag{4.3.2}$$

Where ε is void fraction in the DCC and A_d is interfacial droplet area per volume. The void fraction inside the DCC is equal to 1 because there is no packing or void space.

Spacing between spray nozzles and the narrow column diameter lead to droplet coalescence. Droplet coalescence can happen anywhere inside the DCC when droplets come into close proximity to each other. Drop coalescence rate increases with an increase in holdup because the likelihood of collisions is increased. The spray hits the column wall and rebounds back into the radial direction increasing the likelihood of a collision. Droplet coalescence limits the efficiency of the DCC because the event of contact between aerosol particles (~10 [µm]) and droplets (~100-200 [µm]) is decreased. As described in Section 3.3 an experiment was designed to obtain an estimate of the droplet size observed in the DCC.

5. Results

5.1. Experimental Log

Data was collected for 8 separate trials. The experimental log of all trials is shown in Table 5.1.1.

Table 5.1.1: *Experimental Log of All Trials in Iowa*
Experimental log of all trials conducted in Iowa. Trials 1-5 were conducted on Day 1 and 6-8 were conducted on Day 2. Day 1 was dedicated to experimental equipment setup and construction.

Trial	P_{MW} [kW]	v_{belt} [in/min]	N [#]	W_{hay} [in]	D_{hay} [in]	$\dot{m}_{spraybar}$ [kg/min]	Hay Type	Comments
1	30	30	16	15	2	Off	Wet	Steam emitting out microwave top vents. No steam condensed.
2	30	30	8	15	2	Off	Wet	No steam entering DCC.
3	20	12	8	15	2	Off	Wet	Many arcs and fire. Power increase to 40 [kW]. Mint smell in cooling water tank.
4	35	12	16	15	2	1.1	Dry	DCC exhaust open to surroundings. Many arcs and fires. Power increase to 60 [kW].
5	60	12	16	24	2	1.1	Dry	No arcs after "load" placed in microwave cavity.
6	60	12	16	24	2	1.1	Dry	Blower moved to top of cavity. Re-ran "mint-saturated" cooling water from Trial 5.
7	60	12	16	24	2	1.1	Dry	Fresh water in DCC reservoir. Scale non-operational.
8	60	12	16	24	4	1.1	Dry	Fresh water in condenser tank. Scale non-operational.

Trials 1, 2, and 3 showed that peppermint oil could be extracted from “wet” plant material with a microwave, which had not been done previously. Data from Trials, 1, 2, and 3 was not used for quantitative analysis. During these trials the system was either not producing enough steam, dielectric arcs limited run time, or measurement probes were malfunctioning. However, those trials informed process parameters that were used to produce quantitative data in later trials. Trials 4 through 8 utilized “dry” plant material because the amount of “wet” plant material was limited. The “dry” plant material MC was increased using the spray bar.

Each experimental trial and associated steady state temperature is shown in Table 5.1.2.

Table 5.1.2: *Steady State DCC Inlet Temperature for Experimental Trials*
Steady state temperature at the DCC entrance for experimental trials conducted in Iowa. Inlet temperature is less than that of saturated steam (100 [°C]) because ambient air entering the cavity from the open ends of the microwave mixes with the steam created in the microwave cavity. Steady state DCC inlet temperatures were used to calculate the steam mass entering the DCC.

Trial	T_{in} [°C]
4	48.4
5	52.4
6	72.8
7	72.8
8	77.1

The relative humidity (RH) was monitored at the condenser inlet and outlet. The RH probes were only operational on Day 1 of the experimental trials. The RH profile for Trial 5 is shown in Figure 5.1.1.

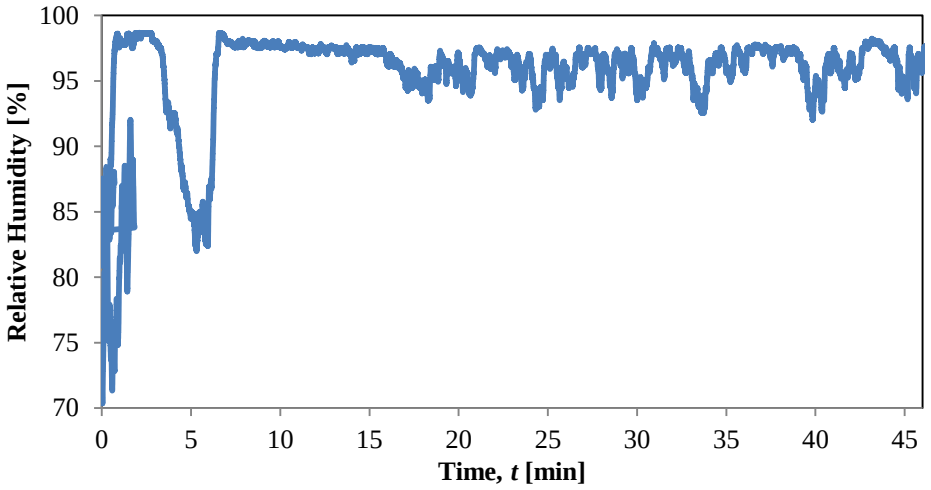

Figure 5.1.1: *Relative Humidity Profile for Trial 5*
Relative humidity (RH) profile for the DCC inlet with 16 nozzles in operation. The decrease in RH from 2 to 5 minutes was a result of the blower being turned off during that time period. The RH probes were only operational during Day 1 of experimentation. The DCC inlet probe was nonoperational. The RH probes were property of Cellencor™, and could not be fixed by the OSU research team.

The moisture content (MC) of a peppermint sample from Trial 4 was determined before and after extraction. The MC before extraction for a sample of "dry" peppermint hay was approximately 33 [%] for Trial 4. The MC post extraction was approximately 4 [%]. The MC was not measured for other trials. Qualitative observation of the brittle, dry mint hay departing the system was performed and suggested consistency with the MC results.

The cooling water from Trial 5 was left to cool overnight, and used again in Trial 6 to increase the concentration of peppermint oil in the cooling water reservoir. The exhaust ports were also opened to the room for Trials 4 through 8 to increase DCC throughput and to better imitate experiments conducted by Lebsack *et al.*

Condenser inlet temperature (T_{in}), outlet air exhaust (T_{exit}), and cooling water ($T_{cooling}$) were continuously monitored during each experiment. Temperature profiles for Trials 5 and 6 are shown in Figure 5.1.2.

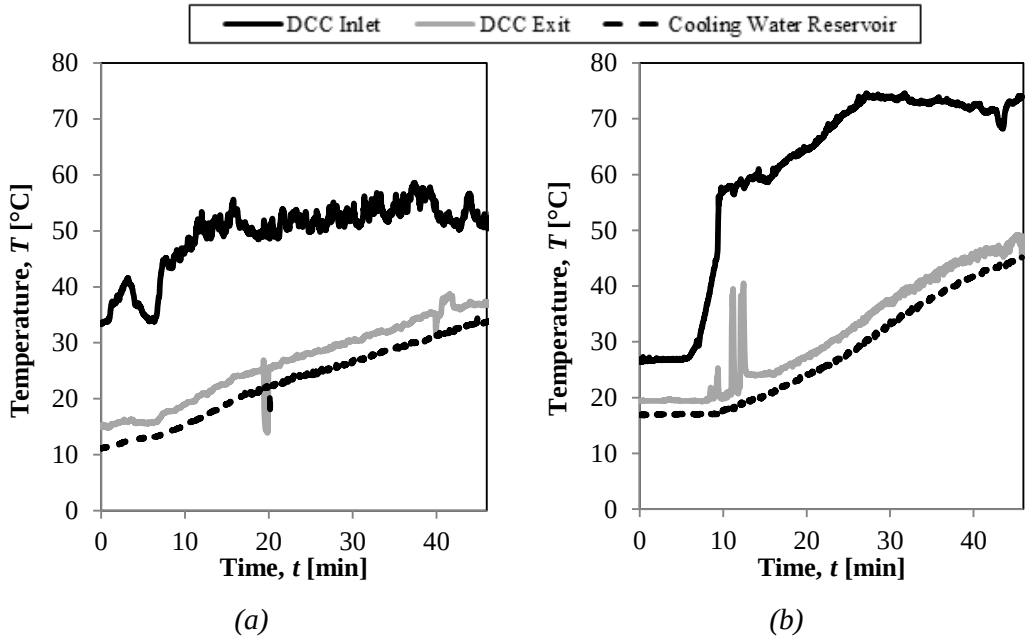

Figure 5.1.2: *DCC Temperature Profiles, Trials 5 and 6*
(a) DCC temperature profile with 16 nozzles in operation and blower on bottom of the microwave cavity. Microwave generator was turned on at t = 0 [min] and DCC was turned on at t = 5 [min]. DCC inlet reached steady state near 52 [°C] around t = 12 [min]. Rapid increase in DCC inlet near t = 8 [min] due to applied microwave power increase. *(b)* DCC temperature profile with 16 nozzles in operation and blower on top of the microwave cavity. Spikes seen in the DCC exit data around t = 12 [min] are due to operators plugging the exhaust port out of the DCC. Microwave generator was turned on at t = 0 [min] and DCC was turned on at t = 9 [min]. DCC inlet reached steady state near 72 [°C] around t = 27 [min]. Rapid increase in DCC inlet around t = 7 [min] due to applied microwave power increase.

Measureable amounts of peppermint oil were not obtained during the trials in Iowa. Water in the recycled cooling tank had a "minty" scent after each trial. Attempts were made to re-run "saturated" cooling water for additional trials to try to reach a measureable amount of peppermint oil in the condensate recycle reservoir. The addition

of a chiller or refrigerating unit would be required to allow continuous recycle of the same mint oil saturated cooling water for longer than the 45 [min] run times.

5.2. Spray Nozzle Droplet Size

Droplet size of a Lechler 460 full cone spray nozzle was estimated using a high speed camera and a standard metric ruler. This technique is a mostly qualitative exploration of the droplet behavior and provides valuable insight into the physical transport phenomena occurring inside of the DCC. Photographs of the spray are shown in Figures 5.4.1, 5.4.2, and 5.4.3.

Figure 5.2.1: *Spray Photograph - Angle View*
120° full cone spray from a Lechler 460.528 spray nozzle from an angled viewpoint captured by a high speed camera. There is clearly a droplet size distribution, as evidenced by this photograph. Droplets are coalescing and splitting apart simultaneously.

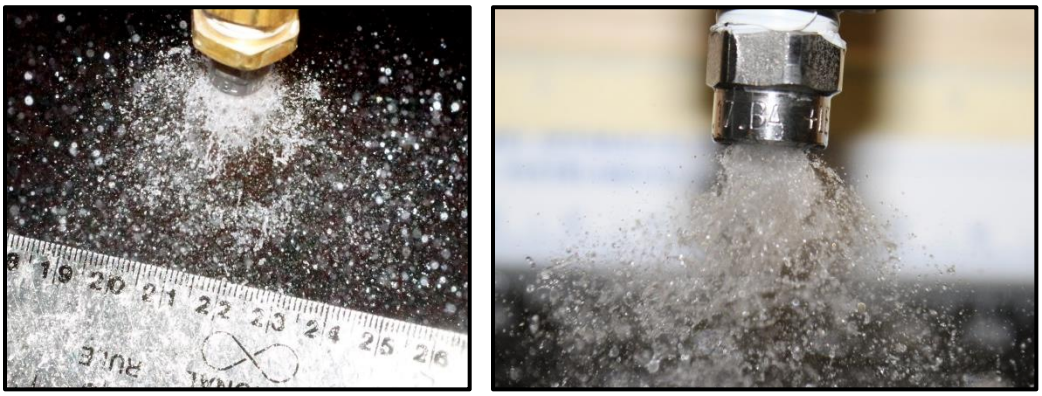

(a) *(b)*

Figure 5.2.2: *Lechler 460.528 Full Cone Nozzle Spray Detail*
(a) Overhead view of spray captured with high speed camera. Droplet size distribution is clearly evidenced by many different droplets coalescing and mixing. *(b)* Spray appears to be very turbulent at the exit from the barrel of the nozzle, as evidenced by the milky water exuding from the barrel. The flow of water dissipates and atomizes into an array of droplet sizes as the distance from the nozzle exit increases. Faucet outer diameter is approximately 13 [mm] for reference.

The spray atomizes as it exits the nozzle barrel to create a distribution of droplet sizes. The estimated average drop size from the photographs is anywhere from 200 to 1000 [µm]. This qualitative range is in agreement with the manufacturer supplied SMD (261 [µm]). The aerosol created in the microwave is assumed to be on the order of 10 [µm]. The goal of the DCC is to increase the surface area available for heat and mass transfer to effectively contact the aerosol as it passes through the 16 spray nozzles. Fluid viscosity and interfacial surface tension affect the ability of the spray condenser. Viscosity and surface tension are functions of temperature. The current system lends itself to an unsteady state process in terms of the viscosity and surface tension of the fluid as an experimental trial progresses. Modeling of the mass and heat transfer between droplets and aerosol particles inside the DCC column and shell would be very helpful to determine the effectiveness of knockdown, but is not explored in this work.

5.3. Condenser Recovery Efficiency

Condensate mass was measured for Trials 4, 5, and 6 after which the scale was not operational. The industrial capacity scale was owned by Cellencor™ and unfortunately

could not be fixed. Condensate mass was extrapolated based on the amount of steam present at the DCC inlet relative to Trials 4, 5, and 6.

Steam mass flow into the DCC, $\dot{m}_{steam,in}$, was calculated from the enthalpy of vaporization, specific heat capacity, temperature difference, and microwave power applied as defined in Equation 4.2.5. Steam mass flow was also verified using hay mass flow and MC measurements to determine a maximum possible steam flow based on water entering the microwave cavity. Microwave power applied in all trials was 60 [kW]. Enthalpy of vaporization was determined based on DCC inlet temperature. The energy balance and condensate mass flow data is presented in Table 5.2.1.

Table 5.3.1: *DCC Energy Balance Data and Condensate Mass Flow*
DCC inlet temperature, ambient temperature, DCC inlet steam mass flow, and condensate mass flow for experimental trials conducted in Iowa. Maximum steam mass flow based on plant material MC was 27.1 [g/s]. Microwave power applied in all trials was 60 [kW]. Condensate mass flow was extrapolated for Trials 7 and 8 based on the specific humidity at the DCC inlet. Extrapolated values are italicized.

Trial	T_{in} **[°C]**	$T_{ambient}$ **[°C]**	$\dot{m}_{steam,in}$ **[g/s]**	$\dot{m}_{condensate}$ **[g/s]**
4	48.4	23	22.3	1.8
5	52.4	23	22.1	3.5
6	72.8	24	21.2	5.5
7	72.8	24	21.2	*8.9*
8	77.1	24	21.0	*10.8*

Specific humidity values at the DCC inlet were calculated for each trial based on the steady state inlet temperature in Table 5.1.2. Condenser recovery efficiency was calculated using Equation 2.4.5.

$$\eta = \frac{m_{condensate}}{m_{steam}} \tag{2.4.5}$$

Values for condensate mass and steam mass are cumulative values for each trial during steady state operation. The condenser would be considered perfectly efficient if all of the steam delivered to the DCC was condensed. Condenser recovery efficiency is plotted versus inlet steam percentage by mass in Figure 5.2.1 for different experimental conditions and condenser types.

Condenser recovery efficiency is plotted versus inlet steam percentage by mass in Figure 5.2.2 for different experimental conditions and condensers.

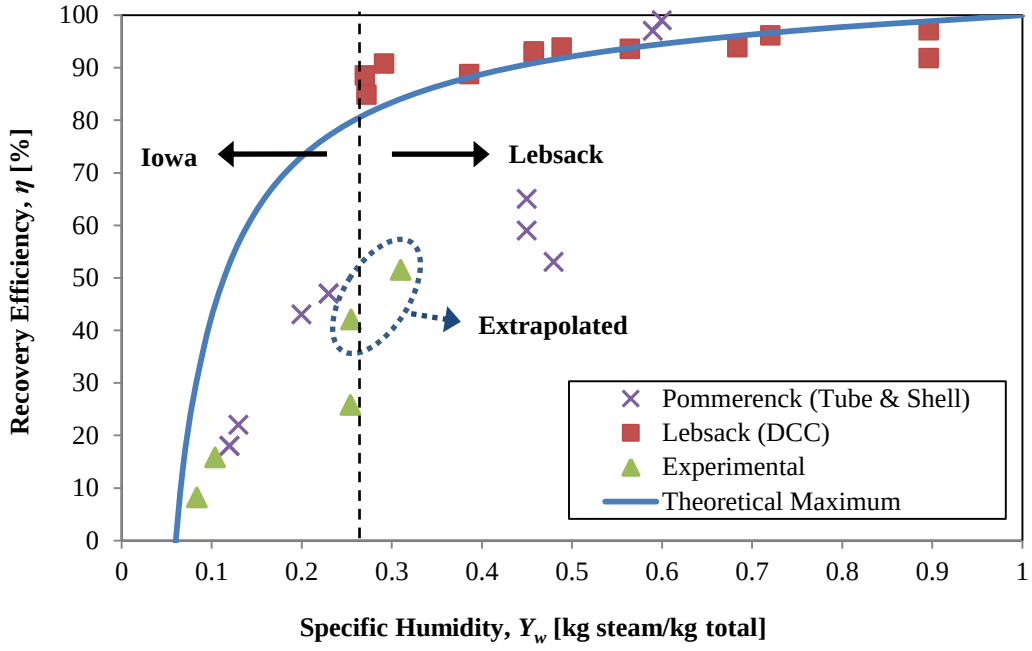

Figure 5.3.1: *Condenser Recovery Efficiency Comparison*
Recovery efficiency of tube and shell and direct-contact condensers plotted versus specific humidity. Recovery efficiency improves with increasing amounts of steam, as predicted by theory. Maximum efficiency observed during experimentation in Iowa was approximately 51 [%]. Air present in the system decreased the efficiency of the DCC, leading to results within a factor of 2 of the theoretical curve. Data for Lebsack and Pommerenck was taken from the respective sources.[30,8] The same DCC used by Lebsack *et al.* was used for the experimental trials conducted in Iowa. A significant decrease in efficiency was observed for specific humidities < 0.3 compared to the results of Lebsack *et al.* The figure depicts two regimes, the regime that Lebsack *et al.* tested (high Y_w) and the regime observed from the Iowa trials (low Y_w). The data points circled in the figure were extrapolated using the condensate mass from Trials 4, 5, and 6 due to the failure of the industrial capacity scale.

Trials conducted in Iowa appeared to operate in a different specific humidity regime than the tests conducted by Lebsack *et al.* and DCC recovery efficiency was within a factor of 2 of the results seen by Lebsack *et al.* DCC recovery efficiency was comparable to the data compiled on a tube and shell condenser studied by Pommerenck *et al.*

Condensate mass flow was compared between Lebsack *et al.* and the data from pilot-scale trials in Iowa and is shown in Figure 5.3.2.

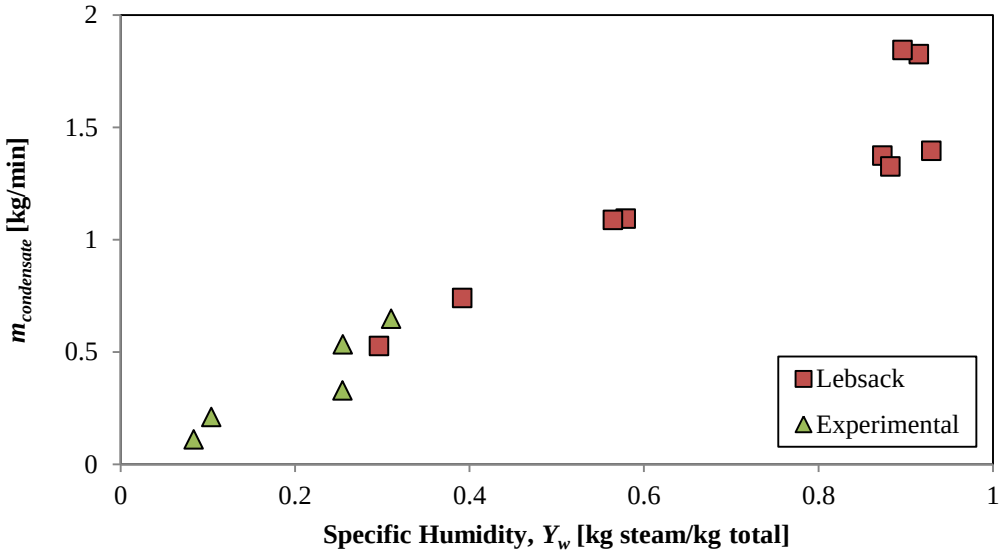

Figure 5.3.2: *Condensate Mass Flow Comparison*
Condensate mass flow of the DCC during experimental trials. The mass flow of condensate linearly increases with increasing specific humidity. The experimental data gathered in Iowa appears to follow the same line of operation as that obtained by Lebsack *et al.* in the lab testing.

Condensate mass flow data indicate that the DCC was operating as predicted by Lebsack *et al.*, where recovery efficiency data indicate that the DCC was not operating as predicted by Lebsack *et al.* Volumetric flow of vapor inlet to the DCC from the microwave process could have been too large, leading to a decreased residence time of the vapor in the DCC unit. Vapor velocity exiting the DCC from one air exhaust port was approximately 7.5 [m/s] for the trials conducted in Iowa. Vapor velocity exiting the DCC from one air exhaust port was approximately 2.0 [m/s] for the Lebsack experiments. The 3-fold increase in vapor velocity could correspond to a decrease in residence time for the vapor inside of the DCC unit. The decrease in residence time could correspond to the decrease in capture efficiency seen in Iowa. Vapor velocity exiting the DCC in Iowa was larger than that of Lebsack *et al.* because steam would have escaped out of the open ends of the entrance and exit to the microwave if the blower was not set to maximum speed.

6. Discussion and Conclusion

6.1. Overall Observations

The microwave system effectively created steam from existing water in the plant material for both “wet” and “dry” peppermint hay. Previous to the studies conducted in Iowa, microwave extraction of freshly cut (“wet”) peppermint had not been performed. The potential for this application would obviate chopping and decrease operation cost and harvest time.

Experimental trials were limited in time based on the cooling water reservoir temperature. Each experiment lasted approximately 45 [min]. There was no measureable amount of mint oil recovered from the trials in Iowa. The recycled cooling water reservoir smelled “minty” after each trial, indicating that some of the mint oil was condensed by the DCC. It was proposed that the saturation of mint oil in the cooling water was never reached during the experiments in Iowa. Sufficient saturation of the cooling water would be required before recycling the cooling water stream during experimentation in the future. A reservoir of water containing a significantly greater volume than the current system or chiller would need to be inserted into the process to increase extraction times. Maintaining a reasonable temperature difference between the incoming steam and the recycled cooling water is critical to efficient heat transfer. Inserting a chiller decrease the overall energy efficiency of the process, which is currently an advantage of microwave extraction when compared to traditional steam distillation. Recycling cooling reduces water usage for the entire distillation process.

DCC aerosol capture was investigated through bench top droplet experiments. Droplet sizes were qualitatively observed to be within the 200-1000 [μm] range. One plausible explanation for limited capture of essential oil was that the droplets from the spray nozzles on the DCC were not contacting the vapor mixture as expected. Further modeling of the droplet and aerosol contacting process would provide more quantitative information in terms of improving the process, but is beyond the scope of this work.

6.2. DCC Recovery Efficiency

There is potential for continuous operation up to 20 [hrs/day] for the entire harvest season (2 to 3 weeks) with the microwave extraction process. However, the issue with industrial-scale implementation of the process is inefficient steam condensation in the presence of air. The DCC recovery efficiency was below the theoretical maximum for the trials conducted in Iowa. Recovery efficiency results of this study combined with that of Pommerenck *et al.* seem to follow a different line of operation (Figure 6.2.1).

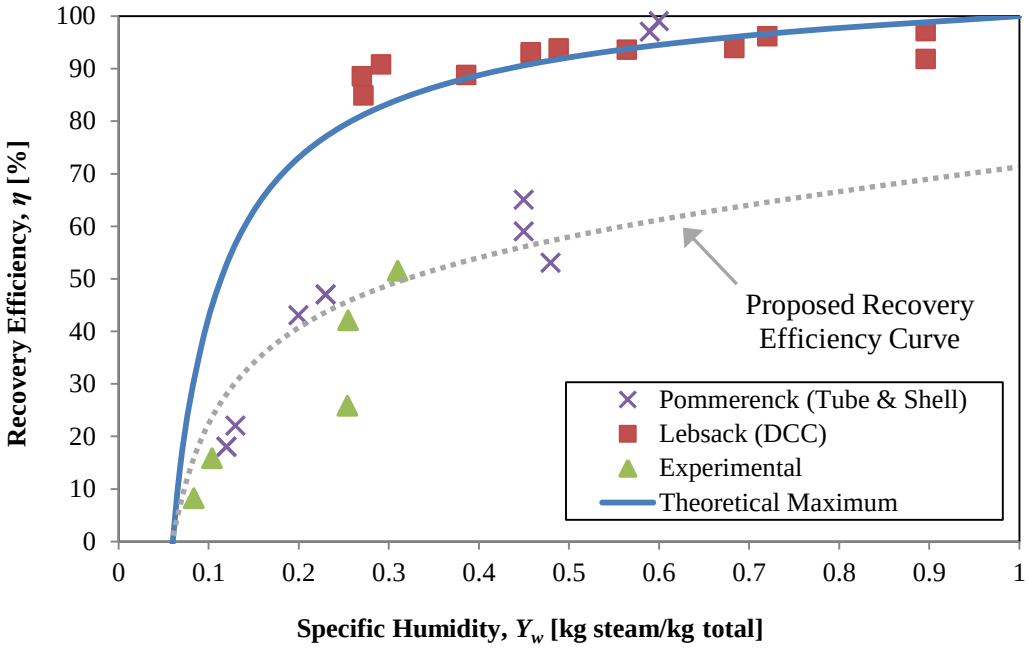

Figure 6.2.1: *Proposed Recovery Efficiency Curve*
Recovery efficiency of tube and shell and direct-contact condensers plotted versus specific humidity. Observed recovery efficiency under experimental conditions in Iowa lead to the proposed recovery efficiency curve. The proposed curve matches up well with most of the Pommerenck *et al.* tube and shell data points at low specific humidity values.

Maximum recovery efficiency in Iowa was 51 [%]. DCC recovery efficiency for the Iowa trials was within a factor of 2 of the theoretical maximum efficiency, which is reasonable for a scaled-up process. The theoretical curve also assumes a perfect process, implying that the results seen in Iowa are promising. Possible explanations for the deviation from the theoretical results include but are not limited to:

1. The direct-contact condenser unit may not have been able to maintain effective aerosol knockdown with the throughput capacity of the microwave system (even though it was designed for a system of that scale).
    a. The number of spray nozzles and associated cooling water flow were insufficient.
    b. Condenser column length may not have been sufficient.
2. Cooling spray and aerosol particles could have traveled through the unit too quickly, not reaching the required residence time for efficient contact, leading to entrapment in the passing air and passage through the DCC exit.
    a. Decreasing blower volumetric flow and thereby increasing aerosol residence time within the DCC could have lead to higher capture rate. However, some of the aerosol would have escaped out of the open ends of the microwave.
3. Steam could have been condensed in the air, creating a "fog" of liquid aerosols entrained in air, instead of vapor aerosols as was assumed initially.
    a. Condensed liquid would require a physical knockdown technique, not condensation, thereby reducing energy costs related to heat transfer.
4. The DCC only deals with gravitational separation. Introducing centrifugal acceleration with a cyclonic separation unit could lead to increased capture efficiency.
    a. Centrifugal acceleration of the aerosol particles could increase the force available for separation of the condensed steam and oil from the air.
5. Other thermodynamic and/or transport phenomena are not being considered.

Scaling up the DCC size, both in volume (pipe and shell dimensions, nozzle location and number) and cooling water throughput capability could potentially improve the efficiency. Experiments conducted by Lebsack *et al.* utilized a homemade steam generation hood and a single speed low capacity fan. Those experimental conditions were not necessarily indicative of what was encountered with the full-scale system. The condenser was also altered before experimentation in Iowa, with the exhaust ports increasing in diameter from 1.5 [in] to 3.5 [in]. This could have impacted the efficiency of the device in terms of aerosol entrapment in the air stream leaving the DCC.

7. Future Work

Significant improvements can be made to the condenser used for continuous SFME processes. Mathematical modeling of steam condensation in the presence of air and the associated mass and heat transfer limitations could provide important insight for the next steps to be taken to improve the viability of the process.

Implementing a physical knockdown technique, instead of a condensation process, could lead to improved capture of mint oil and decreased energy usage. A hypothesis of the trials conducted in Iowa was that the steam was condensing in the air, and creating aerosols of condensed water (and mint oil) droplets. The aerosol could be physically "knocked down" with the appropriate separation technique and equipment.

Additionally, a condenser built specifically for the outlet fittings on the microwave cavity would also be beneficial. There were several manual modifications made to the DCC in Iowa that could have decreased capture efficiency. Pipe dimensions, condenser cavity volume, and spray nozzle locations should be considered in the new design.

7.1. Cyclone

Cyclonic separation is the most widely used physical knockdown technique for separation of particulates and air.[5] This method would be more energy efficient than a "condenser" because it does not rely on a temperature difference as the driving force, but mechanical inelastic collisions. Surface properties of the fluids will be important to minimize elastic collisions. Fluid design will be important to direct fluid particles into a receiving/collecting region. Extensive mathematical modeling, design calculations, and experimentation would be required before implementation of the cyclone into another pilot-scale test. General liquid-phase contacting cyclone schematics are shown in Figure 7.1.1.

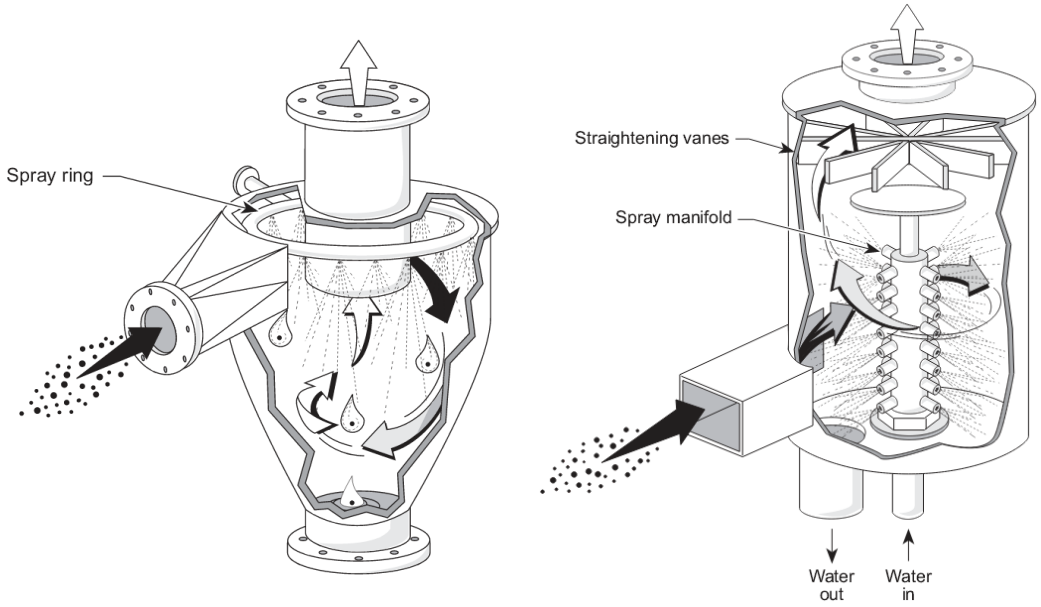

Figure 7.1.1: *Liquid-Phase Contacting Cyclone Separators*
(a) Irrigated cyclone scrubber used by the U.S. Environmental Protection Agency (EPA). Gas enters the chamber tangentially through the top, travels down the conical wall, and leaves through the central opening at the top of the unit. The condensed liquid is separated at the bottom of the unit. Spray ring is mounted at the top of the conical chamber to contact the gas. *(b)* Cyclonic spray scrubber used by the U.S. EPA. Gas enters the chamber tangentially at the bottom, travels up the walls, and leaves through the central opening at the top of the unit. The condensed liquid is separated at the bottom of the unit. The spray manifold is mounted to a center post and directed toward the gas.[5,55]

The operating conditions commonly used for cyclones introduce centrifugal acceleration values ranging from 5 to 2500 times gravity depending on the size and application of the unit.[5] Liquid droplets are forced to the walls of the cyclone and removed from the gaseous stream. However, cyclones decrease in efficiency with particle diameters less than 5 to 10 [μm], the size of the aerosol in this study.[5] Separation could be aided by the addition of baffles to the units pictured in Figure 7.1.1. Baffles increase residence and contacting time between the spray and the passing gas. The particle diameter where 50% of particles are collected, $D_{p,th}$, is defined by Equation 7.1.1.

$$D_{p,th} = \sqrt{\frac{9\mu_g D_c}{4\pi N_s v_{max}(\rho_p - \rho_g)}} \tag{7.1.1}$$

Where μ_g is gas viscosity, D_c is cyclone chamber diameter, N_s is effective number of spiral paths taken by the gas within the body of the cyclone, v_{max} is either inlet or outlet maximum velocity, ρ_p and ρ_g are particle and gas density, respectively. Cyclone efficiency, E_o, is directly proportional to $1/D_{p,th}$ as shown in Equation 7.1.2. [5]

$$E_o \propto \frac{1}{D_{p,th}} = \sqrt{\frac{4\pi N_s v_{max}(\rho_p - \rho_g)}{9\mu_g D_c}} \quad \rightarrow \quad E_o \propto \sqrt{\frac{(\rho_p - \rho_g)}{\mu_g}} \qquad (7.1.2)$$

Fluid properties are influenced by temperature and pressure of the system. Increases in system temperature will lead to increased gas viscosity and therefore decreased cyclone efficiency. Particle density is assumed to be much greater than the gas density for most cyclonic separation systems. The collection efficiency is plotted versus normalized particle size in Figure 7.1.2.

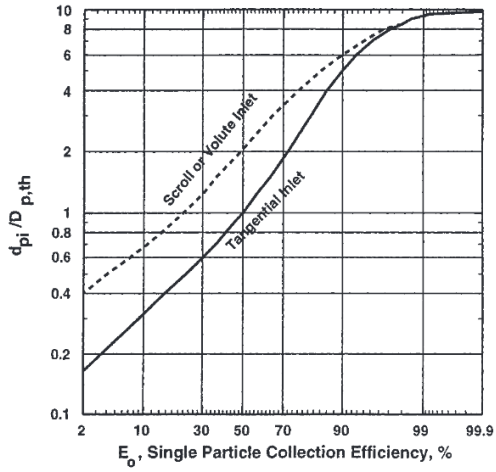

Figure 7.1.2: *Cyclone Collection Efficiency*
Cyclone collection efficiency plotted versus normalized particle size.[5] The single particle collection efficiency increases with increasing particle size. To apply the cyclone to the microwave extraction system, the aerosol particle size distribution would need to be determined or estimated.

A quantitative aerosol particle size distribution produced by the microwave extraction system would inform the design considerations of a cyclonic separator. Aerosol size distribution could be determined from a TSI® Scanning Mobility Particle Sizer Spectrometer that has a size range of 2.5 to 1,000 [nm].[56] The author directs interested researchers to Section 17 of Perry's Chemical Engineer's Handbook for a more detailed description of cyclonic spray scrubbers and associated design considerations.

BIBLIOGRAPHY

1. Bakkali, F.; Averbeck, S.; Averbeck, D.; Idaomar, M., Biological effects of essential oils – A review. *Food and Chemical Toxicology* 2008, 46, 446 - 475.
2. Hughes, A. D. *Improvements in the Field Distillation of Peppermint Oil*; Oregon State University: Corvallis, OR, 05/23/2013, 1952; p 68.
3. Hayward Gordan Ltd.: Boiler Chemical Feed Systems 101. http://www.haywardgordon.com/usercontent/documents/Boiler_Chemical_Feed_Systems_101.pdf (accessed October 17, 2013).
4. Lucchesi, M. E.; Chemat, F.; Smadja, J., Solvent-free microwave extraction of essential oil from aromatic herbs: comparison with conventional hydro-distillation. *Journal of Chromatography A* 2004, 1043, 323 - 327.
5. Perry, R. H.; Green, D. W., *Perry's Chemical Engineers' Handbook*. 8th ed.; McGraw-Hill: New York, NY, 2007.
6. Hackleman, D. *Solvent Free Microwave Extraction of Peppermint Oil - August 2009 Field Trial Report*; Oregon State University: 2009.
7. Hackleman, D. *Microwave Field Test Project - Field Trial Report*; Oregon State University: 11/20/2009, 2009.
8. Lebsack, J. Efficiency of a Direct Contact Condenser in the Presence of the Noncondensible Gas Air Compared to a Tube and Shell Condenser. Oregon State University, Corvallis, OR, 2012.
9. Peppermint Production. In *Department of Agriculture, Forestry, and Fisheries - Republic of South Africa*, Directorate Communication Services: Department of Agriculture, Forestry and Fisheries: Pretoria, South Africa 2012; p 2.
10. I.P. Callison & Sons: U.S. Mint Growing Regions. http://www.ipcallison.com/growing.htm (accessed August 20, 2013).
11. Lawrence, B. M., *Mint: The Genus Mentha*. 2nd ed.; CRC Press: Danvers, MA, 2007.
12. Smith, G. Essential Oil Manufacturing in the US Industry Market Research Report Now Available from IBISWorld. http://www.prweb.com/releases/2013/9/prweb11129857.htm (accessed 10/22/13).
13. McConkey, M. E.; Gershenzon, J.; Croteau, R. B., Developmental regulation of monoterpene biosynthesis in the glandular trichomes of peppermint. *Plant Physiology* 2000, 122, 215-223.
14. Sanford, S. *Mint Oil Energy Consumption, Energy Use Efficiency and Distillation Processes: A Review of Essential Oil Extraction Technologies*; University of Wisconsin-Madison: 2011.
15. Lacy, M. L.; Stephens, C. T.; Green, R. J.; York, A. C. *Mint Production in the Midwestern United States.*; Co-operative Extension Service, Michigan State University: East Lansing, Michigan, 1981; pp 1-18.

16. Felder, R. M.; Rousseau, R. W., *Elementary Principles of Chemical Processes*. Wiley: Hoboken, NJ, 2004; p 675.

17. Koretsky, M. D., *Engineering and Chemical Thermodynamics*. 1st ed.; John Wiley & Sons, Inc: Hoboken, NJ, 2004; p 553.

18. Peppermint Oil MSDS. Sigma-Aldrich: St. Louis, MO, 2013; Vol. MSDS No. W284815.

19. Velasco, C. Microwave Extraction of Peppermint Oil and Comparison to the Current Practice of Steam Extraction. Oregon State University, Corvallis, OR, 2007.

20. Wilson, R.; Marcum, D. B.; Klonsky, K. M.; De Moura, R. L. *Sample Costs to Establish a Mint Stand and Produce Peppermint Oil - Intermountain Region*; University of California Davis - Cooperative Extension: 2011.

21. Lathrop, C. M. What is Boiler Horsepower? http://www.farmcollector.com/steam-traction/what-is-boiler-horsepower.aspx (accessed 10/22/13).

22. U.S. Price of Natural Gas Sold to Consumers. United States Energy Information Administration (US EIA): 2013.

23. Weekly U.S. No 2 Diesel Retail Prices. United States Energy Information Administration (US EIA): 2013.

24. Boundy, B.; Diegel, S. W.; Wright, L.; Davis, S. C. *Biomass Energy Data Book*; Oak Ridge National Laboratory: 2011; p 201.

25. Gregory S., e. a. *MIRC Sustainability Strategy: Carbon Footprint Analysis for Mint Farming*; Mint Industry Research Council (MIRC): 2011.

26. US EPA, C. C. D., Glossary of Climate Change Terms. 2013.

27. AMTek Microwaves: Continuous Cooking Systems. http://www.4amtek.com/index.php/products/continuous-cooking-systems/.

28. Hackleman, D. E.; Lebsack, J. M.; Dean, B. OilExTech, LLC. www.oilextech.com.

29. Welty, J. R.; Wicks, C. E.; Wilson, R. E.; Rorrer, G. L., *Fundamentals of Momentum, Heat, and Mass Transfer*. 5th ed.; Wiley: Hoboken, NJ, 2008.

30. Pommerenck, J.; Alanazi, Y.; Gzik, T.; Vachkov, R.; Pommerenck, J.; Hackleman, D. E., Recovery of a multicomponent, single phase aerosol with a difference in vapor pressures entrained in a large air flow. *Journal of Chemical Thermodynamics* 2012, 46, 109–115.

31. Boehm, R. F., *Heat Transfer Handbook*. Wiley: New York, NY, 2003; p 1496.

32. Celata, G. P.; M., C.; F., D. A.; E., F. G., Direct contact condensation of steam on droplets. *International Journal of Multiphase Flow* 1991, 17, 191–211.

33. Cellencor: High Power Microwave Solutions. http://www.cellencor.com/.

34. Industrial Microwave Systems (IMS), Inc. http://www.industrialmicrowave.com/faqs.htm#six.

35. Grainger: Dayton Permanent Split Capacity (PSC) Blower, 115 Volt. http://www.grainger.com/Grainger/DAYTON-PSC-Blower-1TDR3?Pid=search (accessed May 8th, 2013).
36. Allen-Bradley: PowerFlex 4 and 40 AC Drives. http://literature.rockwellautomation.com/idc/groups/literature/documents/td/22-td001_-en-p.pdf (accessed May 8th, 2013).
37. Burns Engineering: FAQ's - and answers from the Temperature Measurement Experts... http://www.burnsengineering.com/faq/ (accessed May 7th, 2013).
38. Automation, R. Allen-Bradley PanelView 600. http://literature.rockwellautomation.com/idc/groups/literature/documents/um/2711-um014_-en-p.pdf.
39. U-Haul: 4x8 Cargo Trailer Rental. http://www.uhaul.com/Reservations/EquipmentDetail.aspx?model=UV.
40. AccuSpray: Broadcoast Spray Nozzles. http://www.accuspray.com/TechPages/pdf/broadcast.pdf.
41. Mettler-Toledo HB43-S Halogen Moisture Analyzer. http://us.mt.com/us/en/home/products/Laboratory_Weighing_Solutions/Moisture_Analyzer/HB43-S_1.html (accessed May 8th, 2013).
42. Lechler Lechler Full Cone Nozzles - Series 460/461. https://shop.lechler.de/is-bin/intershop.static/WFS/LechlerUS-Shop-Site/LechlerUS-Shop/en_US/PDF/02_produkte/industrie/03_Full_Cone_Nozzles/Series_460_461_FullCone.pdf (accessed May 8th, 2013).
43. Flotec: Residential Sprinkler Pump Specification - FP5172-08. http://www.flotecpump.com/ResidentialProduct_fl_lg_sp_FP5172.aspx (accessed May 8th, 2013).
44. Eagle Manufacturing Company: Spill Containment Products - Model 1612. http://www.eagle-mfg.com/spillcon.html (accessed May 8th, 2013).
45. Company, K. P. Clear Vinyl Reinforced Hose. http://kentak.com/clear-vinyl-reinforced-hose.html (accessed May 8th, 2013).
46. Company, Z. P. Sump, Effluent, Dewatering Cast Iron Series 98. http://www.zoellerpumps.com/ProductBenefit.aspx?ProductID=92.
47. Extech Instruments: AN100 CFM/CMMThermo-Anemometer. http://www.extech.com/instruments/product.asp?catid=1&prodid=2 (accessed May 5th, 2013).
48. Vernier Software & Technology, L. Verneir Type K Thermocouple. http://www.vernier.com/products/sensors/temperature-sensors/tca-bta/ (accessed May 7th. 2013).
49. RTD Elements and RTD Probes - Resistance Temperature Detection Sensors(RTDS). http://www.omega.com/rtd.html.

50. Vernier Software & Technology, L. Vernier LabQuest Handheld Interface. http://www.vernier.com/products/interfaces/labq/ (accessed May 7th. 2013).
51. ScaleRite Micro Electronic Industrial Platform Scale. http://www.scalerite.co.za/micro-receiving-scale-a12e.htm (accessed May 8th, 2013).
52. Company, N. M. Pyramid Shaped Oil Receiving Can. http://www.newhouse-mfg.com/Brochures/PYCan.pdf (accessed April 29th, 2013).
53. Shurflo 8000 Series Diaphragm Pump. http://legacy.shurflo.com/pages/new_industrial/industrial/gen_industrial/genind_doc_sum/8000-443-236.html (accessed April 29th, 2013).
54. Lefebvre, A. H., *Atomization and Sprays*. Hemisphere Publishing: New York, NY, 1989.
55. (EPA), U. S. E. P. A., Combination Devices - Liquid-Phase and Gas-Phase Contacting Scrubbers. 1996.
56. TSI, Inc. - Scanning Mobility Particle Sizer Spectrometer 3936. 2013.

APPENDIX

APPENDIX A

A. Condenser Shell Specifications

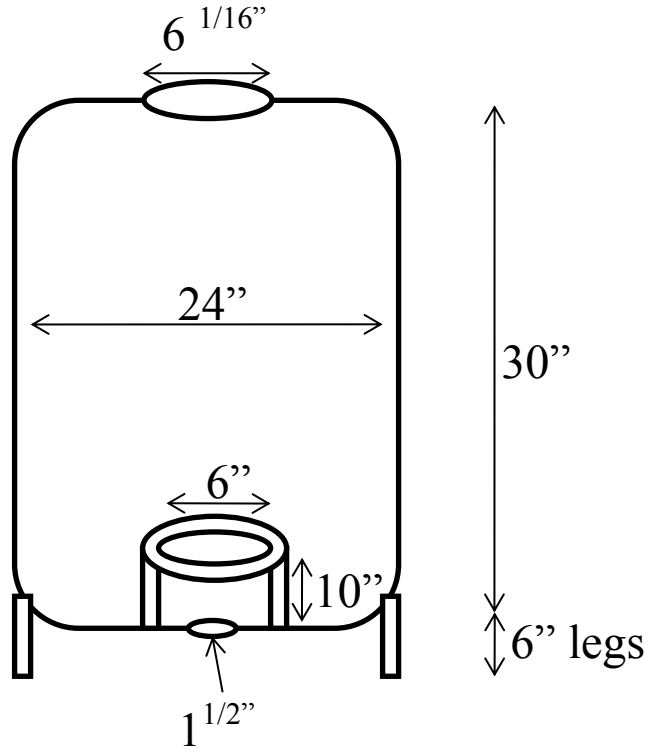

Figure A.1: *DCC Shell Specification - Side View*
Side view of the direct-contact condenser shell. All dimensions should be considered approximate.

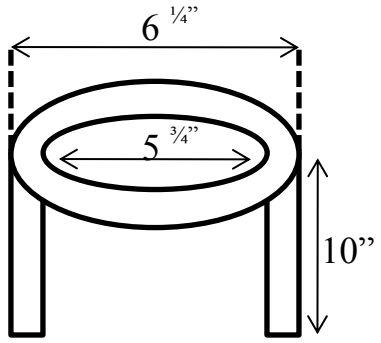

Figure A.2: *DCC Shell Support Platform Specification*
Side view of the direct-contact condenser shell support platform. All dimensions should be considered approximate.

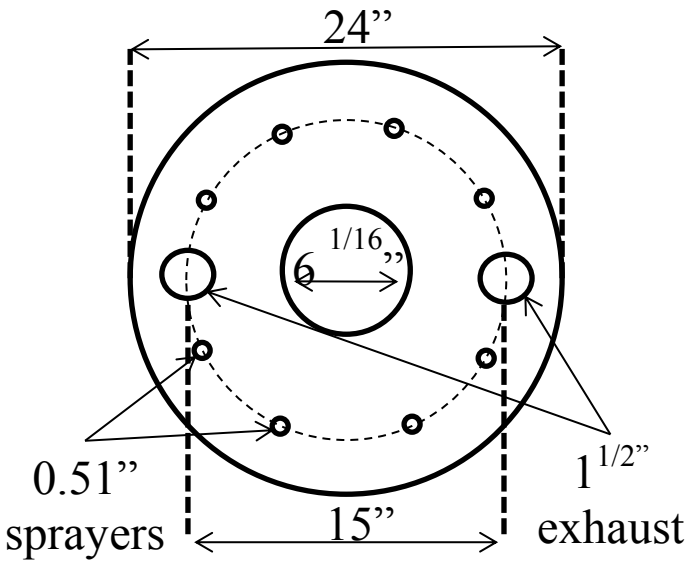

Figure A.3: *DCC Shell Specification - Top View*
Top view of the direct-contact condenser shell. All dimensions should be considered approximate.